The signature of lithospheric anisotropy at post-subduction continental margins: new insight from XKS splitting analysis in northern Borneo

Conor A. Bacon[a,*], Nick Rawlinson[a], Simone Pilia[a,b], Amy Gilligan[c], Deborah Wehner[a], David G. Cornwell[c], Felix Tongkul[d]

*Corresponding author, conor.bacon@cantab.net
[a]University of Cambridge
[b]University of Milano-Bicocca
[c]University of Aberdeen
[d]Universiti Malaysia Sabah

Contacts
C.A. Bacon – conor.bacon@cantab.net
N. Rawlinson – nr441@cam.ac.uk
S. Pilia – simone.pilia@unimib.it
A. Gilligan – amy.gilligan@abdn.ac.uk
D. Wehner – dw545@cam.ac.uk
D.G. Cornwell – d.cornwell@abdn.ac.uk
F. Tongkul – ftongkul@ums.edu.my

The signature of lithospheric anisotropy at post-subduction continental margins: new insight from XKS splitting analysis in northern Borneo

Conor Andrew Bacon[a,*], Nick Rawlinson[a], Simone Pilia[a,b], Amy Gilligan[c], Deborah Wehner[a], David G. Cornwell[c], Felix Tongkul[d]

[a] *Department of Earth Sciences, University of Cambridge, UK*
[b] *Department of Earth and Environmental Sciences, University of Milano-Bicocca, Italy*
[c] *School of Geosciences, University of Aberdeen, UK*
[d] *Faculty of Science and Natural Resources, Universiti Malaysia Sabah, Malaysia*

Abstract

The relative paucity of recent *post*-subduction environments globally has meant that, so far, little is known about tectonic processes that occur during and after subduction termination, as previously convergent tectonic plates adjust to the new stress regime. The region of Southeast Asia that now encompasses northern Borneo has been host to two sequential episodes of subduction—both now terminated—since the mid-Paleogene. It is expected that these processes will have left signatures in the fabric of the upper mantle, which are manifest in the form of seismic anisotropy. We investigate the evidence for, and alignment of, anisotropic fabrics by measuring the splitting of a family of teleseismic shear phases. These observations provide a measure of the orientation of the effective anisotropic elastic tensor, in the form of the orientation of the fast shear-wave polarisation, ϕ, and the strength of the anisotropic fabric, in the form of the delay time, δt. We observe two principal trends across northern Borneo that appear to be confined to the lithosphere, which we relate to tectonic processes associated with subduction, continental collision, and oceanic basin formation, events that can exert primary influence on the formation of post-subduction settings.

Keywords: seismic anisotropy, shear-wave splitting, subduction, post-subduction, Southeast Asia

1. Introduction

Northern Borneo—broadly coextensive with the Malaysian state of Sabah—lies near the north-eastern edge of the present-day Sundaland block, in Southeast Asia (Figure 1). This block, bounded by the seismically active Sunda and Philippines subduction zones, represents the southern extent of the slow-moving (∼20 mm year^{-1}) Eurasian plate [1]. Like much of eastern Borneo, northern Borneo was accreted onto the

*Corresponding author

eastern margin of Mesozoic Sundaland between the Late Cretaceous and the Early Miocene [13]. Though it now exhibits the characteristics of an intraplate setting, there is evidence in the geological record to suggest that it has been host to two opposing subduction systems since the start of the Neogene, both now terminated (see Figure 2). It is widely thought that the proto-South China Sea was subducted beneath the north-west continental margin of northern Borneo—continuing north-east along what is now Palawan—during the Paleogene, before terminating in the Early Miocene with continent-continent collision between the Dangerous Grounds and the north-western margin of Sabah [14, 13, 16]. The lithosphere in this region was probably thickened by underthrusting of the Dangerous Grounds beneath northern Borneo, leading to the formation of the arcuate Rajang-Crocker orogenic belt that runs down the north-west coast of Borneo [16]. This orogenic event was accompanied by a period of rapid uplift mostly across north-western Borneo [25]. At around the same time (∼21 Ma), the Sulu Sea began to open, possibly due to back-arc spreading driven by slab rollback from the northward subduction of the Celebes Sea [13]. Recent geochemical analyses have indicated that an exposed ophiolitic complex around Telupid (central Sabah, see Figure 1) bears the signature of oceanic rifting, with radiometric U-Pb ages dating these basalts to around 9 Ma [surface geology and geochemical dating shown in supplementary Figure S1; 43]. Furthermore, crustal thickness estimates have also revealed a degree of thinning in the crust that coincides with the exposed ophiolite, extending in from the Sulu Sea towards Telupid [30, 12]. Together, these suggest that Sulu Sea rifting propagated into what is now Sabah, but ultimately failed to initiate extensive seafloor spreading. Subduction of the Celebes Sea is thought to end at approximately 9 Ma, based on depletion of arc magmatism in Semporna Peninsula [21]. A series of enigmatic post-subduction processes have since occurred in Sabah. The emplacement of the Kinabalu granite under a NW-SE extensional setting formed the bulk of the 4100 m high Mount Kinabalu, which has been dated to the Late Miocene (between 8 and 7 Ma), before it was rapidly exhumed [5]. Sabah continued to undergo extension, possibly up until the Late Miocene, before it was subsequently uplifted in the Late Miocene to Early Pliocene, becoming fully emerged above sea level by around 5 Ma [14]. The exact cause of this uplift has not been clearly identified, but it is likely to be different between western and eastern Sabah. Possible explanations include Celebes Sea slab detachment [14] or the development of a gravitational instability with subsequent detachment of a lithospheric drip [30] for eastern Sabah, and proto-South China Sea slab detachment or lithospheric delamination from the thickened region beneath the Crocker range for western Sabah [14]. Additionally, a change to ocean-island volcanism has been recorded in Semporna Peninsula at around 5–2 Ma [23]. The tectonic evolution of Sabah from the late Miocene, and exactly how each tectonic event since the Neogene is related, remains a puzzle, with published models

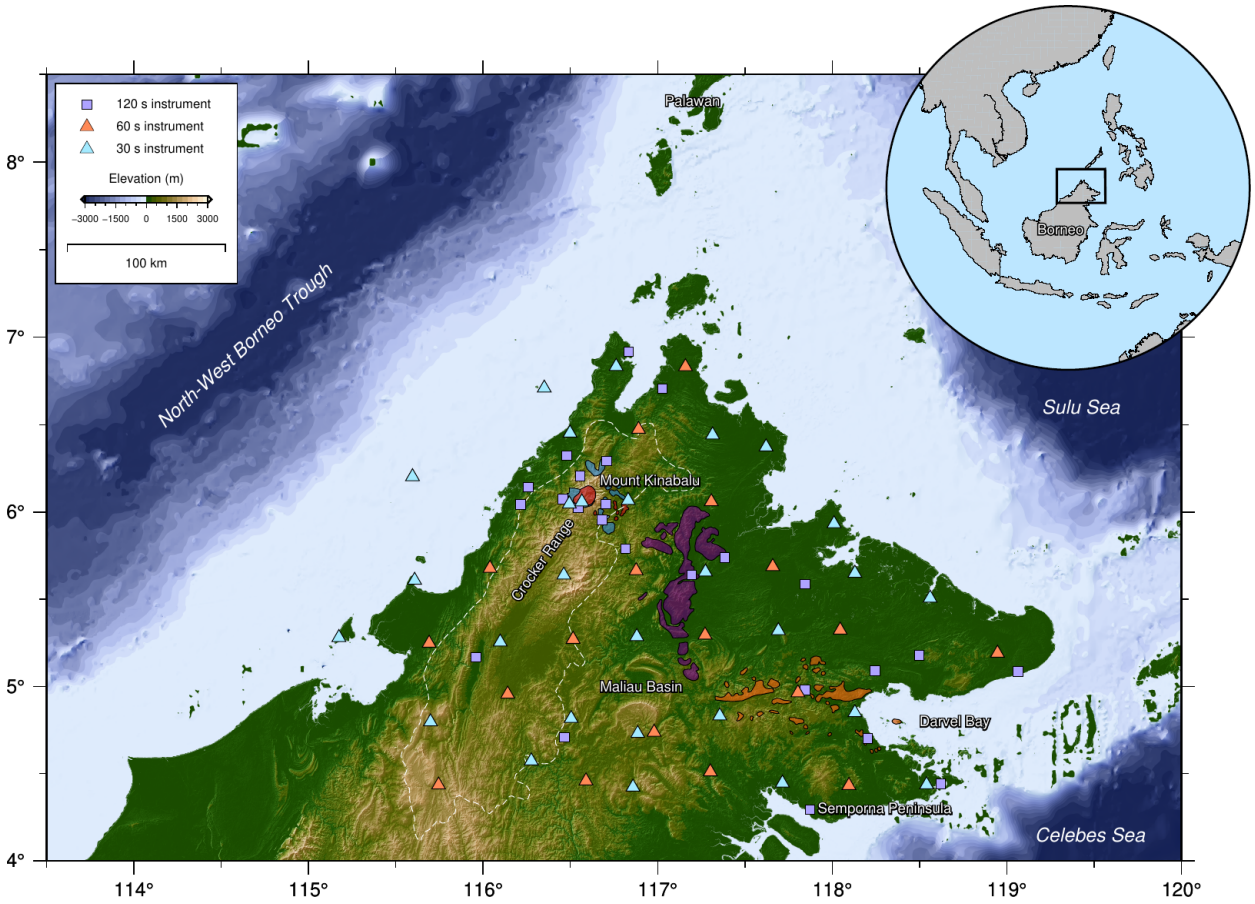

Figure 1: Map of the configuration of the nBOSS network across northern Borneo. Blue and red triangles indicate nBOSS 30 s and 60 s instruments, respectively. Purple squares indicate the permanent broadband stations operated by MetMalaysia. The white dashed line delineates the extent of the Western Cordillera, which encompasses the Crocker and Trusmadi Ranges. A selection of relevant units of the surface geology (derived from Hall [14]) are delineated by shaded polygons: Ranau peridotites (blue), Kinabalu granite (red), Telupid ophiolite (purple), and crystalline basement (orange). A map of the surface geology and a fully labelled network map are available in supplementary Figures S1–2, respectively.

focussing on the crust due to limited constraints on mantle structure and dynamics. Consequently, there exist a number of possible scenarios for variations in the thickness of the lithosphere across northern Borneo and the dynamic state of the asthenosphere below. The region has seen little prior coverage of seismic instrumentation, resulting in a lack of seismic constraints on the structure of the crust and mantle.

Observations of seismic anisotropy—the directional dependence of seismic wavespeeds—have long been linked to deformational processes within the Earth [37]. Provided there exists a relationship between this deformation and the orientation of the induced anisotropic fabric, such observations can be used to make inferences on the dynamic state of the mantle [44], as well as instances of large-scale lithospheric deformation [26, 38]. Under finite strain, intrinsically anisotropic minerals, such as olivine (the primary constituent of the upper mantle), form a preferential alignment with respect to the flow geometry. This allows the intrinsic,

crystal-level elastic anisotropy to manifest on a macroscopic scale, a phenomenon known as lattice preferred orientation (LPO) anisotropy [28, 50]. Under typical mantle conditions, olivine forms A-type LPO, wherein the a-axis of the olivine crystals are aligned parallel to the mantle flow direction. It has been shown, however, that when deformation proceeds by dislocation creep, the resultant LPO is also a function of the physical and chemical conditions (e.g. fluid content, pressure, and temperature) of deformation, which can complicate the connection between observations of seismic anisotropy and the inferred state of the mantle [e.g. 17].

The geometry of mantle flow in active subduction zones has primarily been constrained by measurements of shear-wave splitting in subvertically propagating core-refracted phases, due to their superior lateral resolution compared to surface wave inversions. It is difficult, however, to identify the exact depth of the source of any observed anisotropy, because there may be contributions from different parts of the subduction system, including the overriding lithosphere, the mantle wedge, the slab itself, and the sub-slab mantle. Local S phases originating within the slab can provide useful constraints on the depth distribution of anisotropy

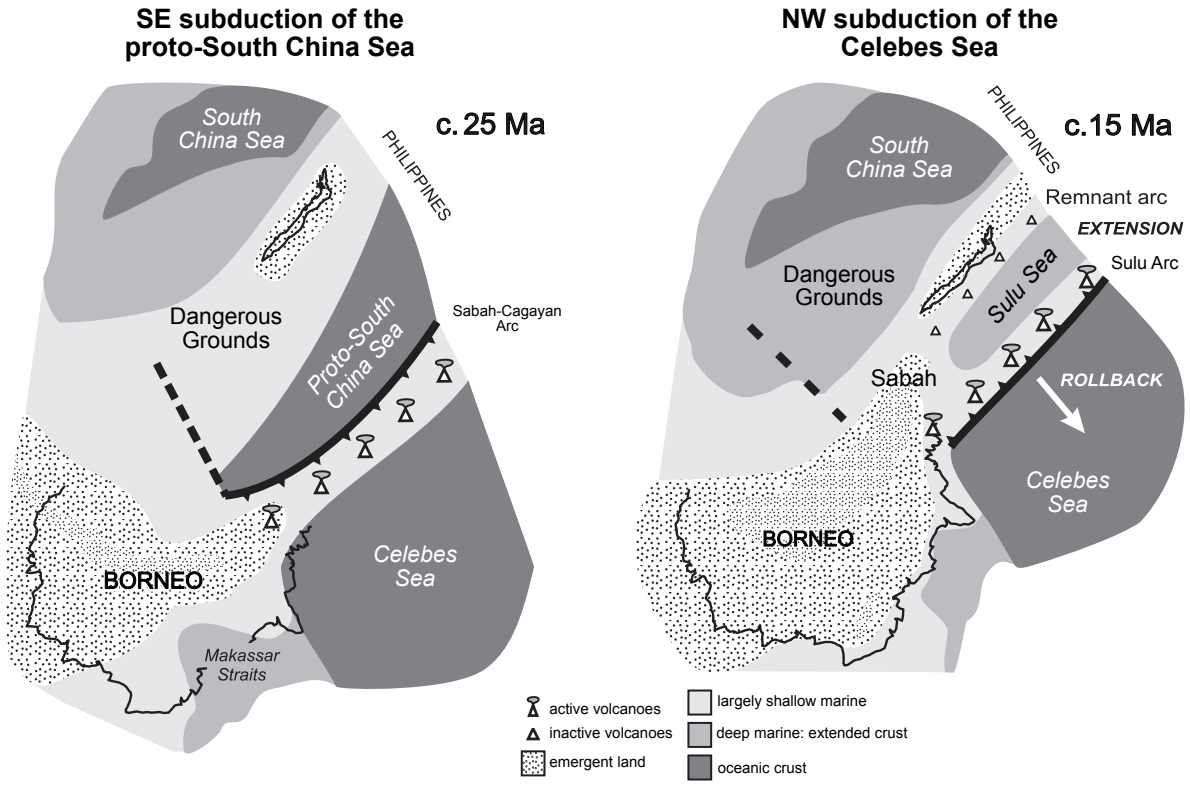

Figure 2: Cartoon showing the two episodes of subduction that have been key to the tectonic evolution of northern Borneo and the Sulu Sea in the late Paleogene and mid-Miocene, modified after [14].

[7, 2]. In the case of Sabah, any remnant lithospheric material in the underlying mantle appears to be entirely aseismic, perhaps as a result of subduction termination and slab breakoff. In general, the anisotropy beneath the mantle wedge in active subduction zones appears to be oriented parallel to the trench [e.g. 33]. In the mantle wedge it is often a more complex picture, with fast orientations tending to be trench-parallel close to the trench and rotating to trench-perpendicular in the back-arc of many systems [18, 9].

In regions undergoing lithospheric shortening, such as northern Tibet, the fast axis of seismic anisotropy tends to be oriented parallel the orogenic belts [e.g. 26, 37, 38, 19], likely as a result of the formation of fabric during the collision that is subsequently frozen into the lithosphere. Observations of shear-wave splitting are therefore useful for not only decoding modern-day mantle flow geometry, but also constraining the tectonic history of continental regions [11, 22].

But what happens *after* subduction stops? How does order established in the upper mantle evolve with the changing stress conditions as the once converging plates cease their relative motion and subduction terminates? Furthermore, what does this mean for seismic anisotropy in systems transitioning from the subduction of oceanic lithosphere to continent-continent collisions and then orogen collapse in a post-subduction environment? Answering these questions will provide fresh insight into the termination and post-subduction phases of the subduction cycle.

Here, we present the first broad-scale study of teleseismic shear-wave splitting using a network of instruments across northern Borneo, with the goal being to understand the present-day dynamics and long-term deformation of the region. The results are interpreted in the context of models that have been proposed for the tectonic evolution of northern Borneo and provide new constraints on the dynamic state of the mantle, particularly the lithospheric mantle, in a post-subduction setting.

1.1. Shear-wave splitting

Shear-wave splitting is a key and near-unambiguous indication of the presence of seismic anisotropy [36, 34]. When a linearly polarised shear wave impinges on an anisotropic medium, it is partitioned into two quasi-S waves, which propagate at different velocities. A time lag, δt, develops between these two waves as they travel through the anisotropic medium, with the final integrated value proportional to both the path length and strength of anisotropy. The polarisation of these two waves, commonly called 'fast' (denoted ϕ hereafter) and 'slow', are controlled by the symmetry and orientation of the anisotropic elastic tensor. The orientation of the fast axis of anisotropy, ϕ, can be related to both present-day asthenospheric flow or historic lithospheric deformation, with the dominant mechanism being LPO of intrinsically anisotropic minerals such as olivine [e.g. 50, 18]. The delay time, δt, is an integrated measure of anisotropy along the raypath, with

a strong trade-off between the thickness of an anisotropic layer and the strength of anisotropy. Studies of azimuthal anisotropy in the upper mantle commonly make use of the family of core-refracted phases that involve a P-to-S conversion at the receiver-side core-mantle boundary (CMB), hereafter collectively referred to as XKS phases [37, 38, 36, 34]. These converted phases are polarised in the radial plane and retain no information on source-side anisotropy—thus, energy observed on the transverse component is diagnostic of anisotropy or lateral heterogeneity beneath the receiver. Consequently, shear-wave splitting measurements provide excellent lateral resolution of seismic anisotropy, but lack vertical resolution.

Though straightforward in theory, the measurement of shear-wave splitting parameters, ϕ and δt, from seismic recordings is made non-trivial by the presence of seismic noise. It is also complicated by the fact that most techniques assume a simple model of anisotropy e.g. a single, horizontal layer. Complex anisotropy, such as multiple anisotropic layers along a raypath, can result in very complicated patterns of shear-wave splitting, though it is possible to deconstruct this by studying how ϕ and δt vary as a function of back azimuth and incident angle [39]. Null measurements are measurements that suggest that there has been no splitting of the wave between the CMB and the receiver. It is possible that these observations indicate that there is no radial anisotropy along the raypath, either due to the Earth being isotropic or because the axis of anisotropy is oriented vertically, which can be the case if there is vertical flow beneath the station [e.g. 47, 24]. In this instance, one would expect to observe nulls at any azimuth. However, null observations may also arise if the initial polarisation of the core-refracted phase is aligned with either the fast or slow axes of anisotropy. The latter case is hereafter referred to as a 'geometric' null and is commonly indicated by null observations being limited to two azimuths, 90° apart. Geometric nulls can still be useful for constraining the orientation of anisotropy, though they (inherently) lack any information on the strength of anisotropy.

2. Data and Methods

The seismic waveform data used in this study were recorded by two networks of seismic instruments (Figure 1): the temporary nBOSS (northern Borneo Orogeny Seismic Survey) network (FDSN network code YC, doi: 10.7914/SN/YC_2018); and the permanent monitoring network operated by the Malaysian meteorological office, MetMalaysia (FDSN network code MY). The nBOSS network, which operated between March 2018 and January 2020, consisted of 46 seismic stations with a mean station separation of 38 km. Two instruments types were used: the Güralp 6TD, a three-component broadband instrument with a flat response between 30 s–100 Hz; and the Güralp 3ESPCD, a three-component broadband instrument with a flat response between 60 s–100 Hz. The MetMalaysia permanent network consists of Streckeisen STS-2/2.5

seismometers, which are three-component broadband instruments with a flat response between 120 s–50 Hz, with their deployment focussing on the seismically active regions around Mount Kinabalu in the north-west and Darvel Bay in the south-east (Figure 1). Restricted data recorded by the MetMalaysia network between January 2018 and January 2020 were made available to the nBOSS working group.

A catalogue of viable events fulfilling the criteria $M_b \geq 5.8$ and epicentral distance $\geq 85^\circ$ was produced, containing a total of 129 earthquakes. A list of the events used in this study and a map showing their location are available in the supplementary information. Model phase arrival times for the XKS phases were calculated using a traveltime lookup table for each event/station pair. Due to the short deployment period, there are notable gaps in the back-azimuthal data coverage (see supplementary Figure S3), which has implications for how the shear-wave splitting measurements can be used for interpreting anisotropic structure. Earthquakes that contributed an observation of shear-wave splitting used in this study are shown as grey circles in the inset of Figure 4.

The MetMalaysia site KKM (see Figure 1c) has been in continuous operation since 2005, with continuous waveform data archived at the Incorporated Research Institutions for Seismology (IRIS) Data Management Center (DMC). A separate catalogue of viable events, using the same criteria, was created in order to produce a long-term benchmark to help validate the observations at the temporary/more recent networks. The distribution of the 1,030 events that are suitable for analysis are shown in the supplementary information and those which contributed an observation of shear-wave splitting used in this study are shown as black squares in the inset of Figure 4. Consequently, the azimuthal coverage at this site greatly exceeds that of any other station in the network, enabling us to investigate the possibility of more complex anisotropic structures beneath Sabah, such as dipping and/or multiple layers, features that might be expected given what is known of the region's tectonic history.

The shear-wave splitting analysis was performed using the SplitRacer code package [32]. All waveform data were bandpass filtered between 3 and 25 s before a signal-to-noise ratio was calculated in a window around the predicted arrival. Only those phase arrivals with a signal-to-noise ratio exceeding 1.5 were retained for splitting analysis. The waveform data were then visually inspected and the automatically assigned analysis windows were assessed. Where necessary, these time windows were adjusted to best capture the phase arrival and exclude any non-XKS arrivals. Poor quality, noisy waveforms were also removed at this stage. The initial splitting analysis was performed using the single channel transverse energy minimisation method of Silver & Chan [37, 38], assuming a horizontal anisotropic layer. This technique consists of a grid search over the two splitting parameters, the fast direction (ϕ) and delay time (δt), to find the combination

that best removes splitting. The uncertainties in the measurements were assessed using the statistical measure laid out in Silver & Chan [38], with the corrections identified in Walsh et al. [45]. The resulting splitting measurements were then visually inspected and classified as 'good' (clear and well-constrained splitting), 'fair' (clear evidence of splitting, but less well-constrained), 'null' (clear absence of splitting), and 'poor' (indeterminable result). Measurements classified as 'poor' were disregarded in further analysis. A measurement was classified as 'good' if it exhibited the following three characteristics: 1) distinct energy on the transverse component prior to correction; 2) elliptical particle motion for the horizontal components before correction, which became rectilinear after correction; and 3) the 95% confidence contour was narrower than 60° along the ϕ axis and 0.25 s along the δt axis, with 'fair' observations exhibiting at least criteria 1) and 2). Additional estimates of ϕ and δt were calculated using the joint analysis method of Wolfe & Silver [48] and the splitting intensity technique of Chevrot [4]. This method incorporates the full suite of information available across multiple observations to maximise the signal-to-noise ratio of the search grids and thus minimise the uncertainties. For the joint analysis, error grids for the good and null observations at each site were stacked and the global minimum extracted. This technique assumes a single layer of anisotropy with a horizontal axis of symmetry, making it prone to inaccuracy in the case of more complex anisotropy, as well as being biased towards event clusters that contribute a large number of good observations. To combat this, the multi-channel splitting intensity method [4] is also used as a means of cross-validating the measured splitting parameters. This technique solves for ϕ and δt at a single station using multiple records from different azimuths simultaneously.

3. Results

3.1. KKM: 2006–2020

Variations in shear-wave splitting parameters as a function of back azimuth are a key indicator of complex, multi-layered and/or dipping anisotropic fabrics. Identification of such patterns, however, is often hampered by the temporary nature of many passive seismic experiments. KKM—a permanent station operated by MetMalaysia since 2005, situated on the north-west coast of Sabah—offers an opportunity to explore potential complex anisotropy. Figure 3a shows the misfit grid resulting from the joint splitting analysis performed at KKM using all single-channel measurements that were previously graded as good or null, which returned a best-fitting (ϕ, δt) pair of (N068°E $\pm$ 4°, 0.92 $\pm$ 0.10 s). There appears to be little to no variation in ϕ as a function of back azimuth (see Figure 3b), which may indicate there is a single dominant horizontal layer of anisotropic material responsible for the shear-wave splitting observed at

Table 1: XKS-wave splitting results for northern Borneo, filtered between 3 and 25 s. See supplementary Figure S2 for station locations. Instrument types are available in the station file provided as part of the supplementary material.

Station Code	**Longitude**	**Latitude**	ϕ	σ_ϕ	δt	$\sigma_{\delta t}$	**n**
SBA3	116.277	4.573	64	5	0.92	0.15	9
SBA4	116.590	4.459	56	21	0.31	0.36	9
SBA5	116.859	4.423	86	5	0.82	0.13	4
SBA7	117.714	4.446	-77	-	null	-	15
SBA8	118.095	4.432	-64	-	null	-	11
SBA9	118.540	4.436	-52	8	0.72	0.28	9
SBB2	115.699	4.798	33	6	0.51	0.18	9
SBB3	116.141	4.956	52	3	1.13	0.10	8
SBB4	116.505	4.817	85	11	0.41	0.13	7
SBB6	117.356	4.832	-70	5	1.13	0.13	12
SBB7	117.803	4.964	-76	23	1.13	0.72	6
SBB8	118.129	4.850	41	-	null	-	9
SBC1	115.175	5.281	46	7	1.23	0.31	3
SBC2	115.692	5.249	50	3	1.33	0.13	10
SBC3	116.099	5.255	55	3	1.23	0.13	10
SBC4	116.516	5.271	60	6	1.03	0.15	5
SBC5	116.881	5.286	-60	15	0.62	0.31	3
SBC6	117.272	5.295	-56	-	null	-	1
SBC7	117.691	5.321	-72	-	null	-	1
SBC9	118.946	5.191	-46	12	0.82	0.36	3
SBD1	115.608	5.609	48	8	1.23	0.31	2
SBD2	116.040	5.677	66	7	0.62	0.15	6
SBD3	116.462	5.639	84	4	1.03	0.13	11
SBD4	116.877	5.664	-72	4	1.03	0.26	9
SBD5	117.274	5.656	75	8	0.82	0.26	5
SBD8	118.560	5.507	-50	-	null	-	4
SBE1	115.596	6.203	68	7	0.72	0.15	4
SBE3	116.831	6.067	38	-	null	-	15
SBE4	117.307	6.060	41	-	null	-	1
SBE5	118.010	5.933	-50	11	2.2	1.03	3
SBF1	116.498	6.452	65	31	0.89	0.21	4
SBF2	116.891	6.474	83	20	1.03	0.50	4
SBF4	117.621	6.373	57	11	1.03	0.38	2
SBG3	117.159	6.832	59	6	0.92	0.33	5
KINA	116.566	6.058	82	9	0.72	0.28	19
MALB	116.980	4.737	65	12	0.41	0.13	9
KAM	116.458	6.074	74	2	0.90	0.27	7
TNM	115.960	5.169	52	14	1.20	0.26	3
TPM	116.260	6.143	63	19	1.41	0.40	6
MTM	116.817	5.789	95	7	0.82	0.37	5
KKM	116.215	6.044	68	4	0.92	0.10	64

KKM (see supplementary Figure S6). In addition to this, the splitting intensity technique was applied to independently measure the splitting parameters, the results of which are shown in Figure 3c. The method returned a strong fit to the data and a best-fitting (ϕ, δt) pair of (N066°E ± 3°, 0.71 ± 0.08 s), which closely agrees with the result of the joint splitting analysis. Together with the limited evidence of back-azimuthal variation, we hereafter treat the anisotropy beneath KKM as simple and perhaps representative of the shear-wave splitting observed at most of the stations along the north-west coast of northern Borneo.

3.2. 2018–2020

A total of 1,437 phase arrivals were analysed, resulting in 687 splitting measurements ranked as 'good' (151), 'fair' (328), or 'null' (208). Examples of good and null observations are shown in supplementary Figure S4 and S5, respectively. From these 687 observations, 271 are from SKS phase arrivals, 353 from SKKS, 37 from PKS, 8 from SKIKS, and 18 from PKIKS. The average delay time for the 'good' and 'fair' splitting measurements is 1.41 ± 0.76 s, which is greater than the global average of 1.0 s for continents [36]. However, this average value may be biased by a small number of stations for which there are a large number

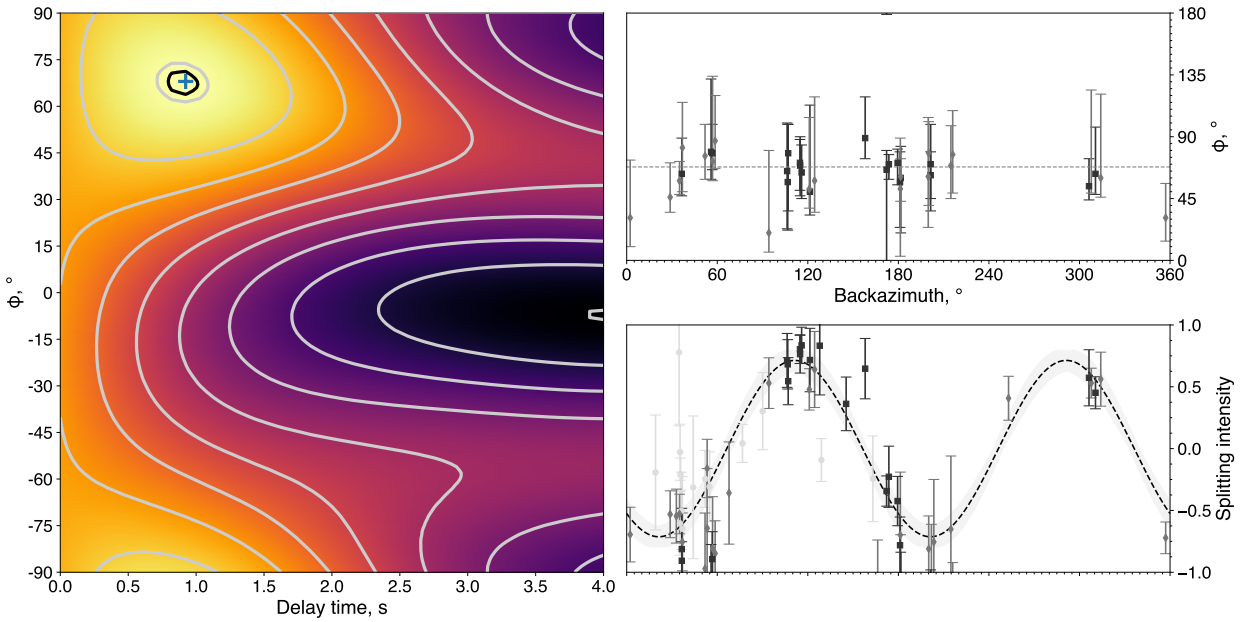

Figure 3: Additional analysis carried out at KKM for the period of 2006–2020. Panel **a** shows the resultant misfit grid from the joint analysis of all good and null measurements at KKM. The black contour represents the 95% confidence interval. The blue plus symbol represents the optimal (ϕ, δt) pair, which is (N068°E ± 4°, 0.92 ± 0.10 s). Panel **b** shows ϕ as a function of back azimuth. The dashed line shows the average ϕ determined from the joint analysis method of Wolfe & Silver [48]. Black squares and grey diamonds represent good and fair measurements, respectively, with corresponding uncertainty measurements. Panel **c** shows the best-fitting splitting vector (dashed line) to observations of splitting intensity. The phase and amplitude of the sinusoid give ϕ and δt, respectively. The black squares and grey diamonds represent the same measurements as in panel **b**. The light grey circles represent null measurements.

of observations. Station misalignments were assessed by comparing the orientation of the first eigenvector of the XKS horizontal particle motion with the back azimuth to the earthquake [e.g. 8]. The average station misalignment was calculated to be -2 ± 5°, which is below the uncertainties of the measured ϕ values for every station (see Table 1) and is in line with the assessment of instrument orientations taken in the field during deployment and retrieval. Stacked results were possible at 42 stations, shown in Figure 4 and listed in Table 1. Taking the average of the joint measurements of δt results in an average delay time of 0.90 ± 0.33 s, which is consistent with the continental average. Two trends in ϕ emerge from the stacked observations. Stations in the west and north-west of Sabah show an average fast orientation of N063°E ± 14°, sub-parallel to the Crocker range and the north-west Borneo trough. In contrast, stations in the east and south-east have an average fast polarisation of N112°E ± 19°, which is sub-parallel to both the Absolute Plate Motion [APM, N120°E; 1] and direction of spreading in the Sulu Sea. A small number of stations, located primarily to the south-east of Mount Kinabalu (see Figure 1), exhibit ϕ values that are perturbed from both the dominant NE-SW and NW-SE trends. Elsewhere, the transition between the two trends appears to be sharp, occurring over $\lesssim$ 40 km.

There are notably fewer measurements in eastern Sabah, despite the uniform network coverage (Figure 1), which may reflect the complex sedimentary successions observed in this area [e.g. 41, 42], as well as an elevated level of noise degrading the phase arrivals. Indeed, the low-lying regions of eastern Sabah are significantly more densely populated than central and southern Sabah. A number of stations exhibit nulls (represented by crosses in Figure 4)—on inspection, it is likely that these are geometric in nature (the observations typically come from a limited back-azimuthal band), as opposed to them indicating that the Earth beneath the stations is isotropic. That aside, there is evidence from mapping of the lithosphere-asthenosphere boundary across northern Borneo that the lithosphere is thinned around Tawau in the south-east of Sabah [30, 12], which is coincident with a number of stations that exhibit nulls (see Figure 4) *and* intraplate volcanism on the Semporna Peninsula [23]. Thinning of the lithosphere can induce vertical flow of the upper mantle, resulting in nulls and, at the very least, disrupting any fossil anisotropy that has been previously frozen in.

There is some variation in δt across northern Borneo, most notably in the south-central region around the Maliau Basin, where there is a notable reduction compared to measurements at nearby stations. This correlates somewhat with the edge of the orogenic belt, but may also be a result of more complex anisotropy as a function of depth beneath this region. However, without sufficient back-azimuthal coverage, it is difficult to be conclusive. Overall, however, there appears to be little variation in ϕ as a function of back

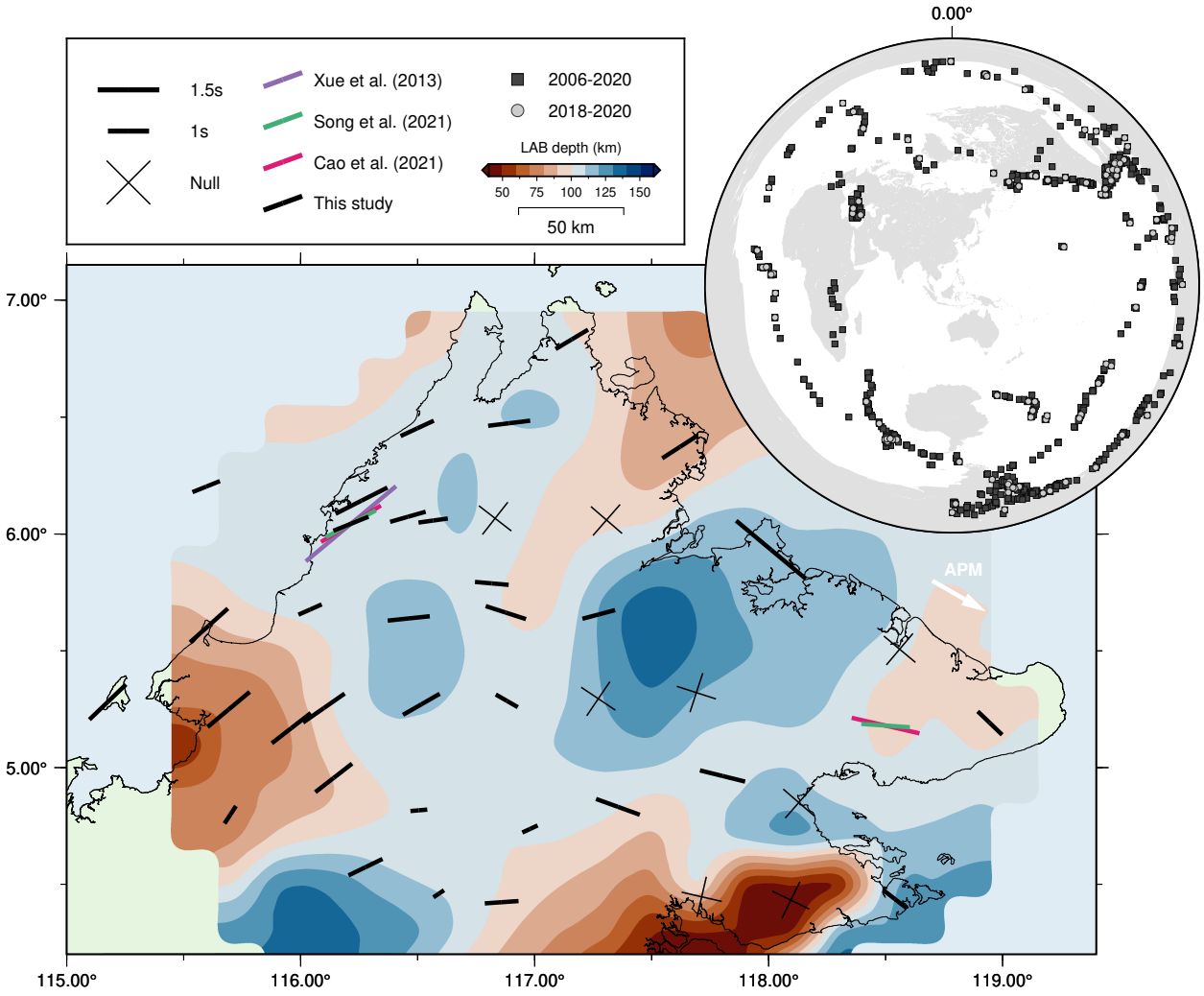

Figure 4: Map of station-averaged XKS splitting measurements from this study (black) and the studies of Xue et al. [49] (purple), Song et al. [40] (green), and Cao et al. [3] (magenta). The white arrow represents the current Absolute Plate Motion which has a bearing of N120°E according to the NNR-MORVEL56 plate model [1]. These results are shown on top of the lithosphere-asthenosphere boundary depth (i.e. the lithospheric thickness) as determined by Greenfield et al. [12]. Supplementary Figures S7–9 show the same results on top of two crustal thickness models and radial anisotropy, derived from a recent FWI tomographic study of Southeast Asia [46].

azimuth, suggesting that a single dominant horizontal layer of anisotropy is sufficient to explain the shear-wave splitting observations [39]. While this is consistent with the conclusions of Song et al. [40], who looked at teleseismic shear-wave splitting at a handful of permanent stations with publicly available data across the Sundaland block, the back-azimuthal coverage is fairly limited for the period between 2018 to 2020 (see inset Figure 4).

4. Discussion

The observed patterns of shear-wave splitting are consistent with the signatures of some of the major tectonic events that have occurred in the last 20 Ma. While the contribution to the observed delay time from the crust cannot be constrained, it has been shown that it typically amounts to around 0.1–0.5 s [36], thus making a mantle contribution necessary to explain our observations. It is possible to estimate the thickness of the anisotropic layer, L, from δt, using the expression $L \approx (\delta t \times V_S)/dV_S$ (where V_S is the shear velocity and dV_S is the average percent anisotropy). Using a V_S of 4.48 km s^{-1} [ak135; 20] and a dV_S of 4% [an upper limit of the degree of anisotropy in the upper 200 km; 34], the mean delay time of 0.9 ± 0.33 s corresponds to a layer thickness of 100 ± 40 km. An estimate of the depth of the lithosphere-asthenosphere boundary beneath the nBOSS network was recently extracted from a shear-wave velocity model, calculated through an inversion for surface wave phase velocities at periods between 25 and 200 s [12, 30]. This study used a two-plane-wave approach and converted from V_S to temperature, before taking the lithosphere-asthenosphere boundary to be the 1333 °C contour (see Figure 4). This model exhibits an average lithospheric thickness of ∼100 km, with notable thinning (∼50 km) around the Semporna Peninsula.

Our results are supplemented by a small number of observations from three previous studies [40, 49, 3], which measure ϕ at the permanent MetMalaysia stations KKM and LDM. The ϕ values measured in these studies are consistent with our value at KKM and with the stations in the vicinity of LDM (see Figure 4). Xue et al. [49] only published a single result at KKM, with a δt significantly larger than that observed in this and other studies [40, 3].

The orogen-parallel trend observed across western and north-western Sabah is strong evidence that the observed seismic anisotropy reflects continent-continent collision between the extended Dangerous Grounds continental margin and the continental margin of northern Borneo, which occurred at roughly 21 Ma. This is consistent with the conceptual framework of vertically coherent deformation [37, 38], in which continental plates deform coherently over their depth extent and can play a significant role in mantle anisotropy. This trend spans the entire area known as the Western Cordillera in Sabah (dashed white line in Figure 1), extends

into the offshore fold-and-thrust belt, and also appears to continue off the northern tip of Sabah towards Palawan. Fast orientations of seismic anisotropy are commonly observed to trend parallel to orogenic belts in continental collision zones, both in the crust [e.g. 10, 29] and in the lithospheric mantle [e.g. 37, 38, 19, 11, 22], with transpression being proposed as the source of strain (through which LPO anisotropy is induced) normal to the relative motion between the two plates [26]. Any fabric within the upper mantle relating to subduction of the proto-South China Sea has likely been overprinted by continent-continent collision. This has implications for the lifespan of anisotropic fabrics within the ductile asthenosphere, suggesting they are much more transient than fabrics left in the lithosphere during large-scale tectonic deformation events.

The mean fast orientation in the east of Sabah is sub-parallel to the APM of the Eurasian plate, though the slow-moving nature of this plate might mean that the relative motion between the plate and the underlying asthenosphere is insufficient to organise the flow within the mantle. In this case, one could discount the dominance of simple asthenospheric flow in controlling the large-scale coherence and alignment of shear-wave splitting observations [36] in favour of an alternative mechanism. While the orientation inferred from our observations of shear-wave splitting is not incompatible with APM-induced LPO anisotropy, the plate velocity is only around 2 cm yr^{-1} [1], which is less than the empirical 4 cm yr^{-1} proposed by Debayle & Ricard [6] as necessary for a plate to organise the flow in its underlying asthenosphere. Hence, it is worth also considering other potential sources for the observed trend, the most prominent among these being the extension and rifting of the nearby Sulu Sea. Until recently, it was believed that northern Borneo was, and still is, under a compressional tectonic regime. However, geochemical analysis of a suite of samples from an ophiolitic complex near Telupid, central Sabah, provided evidence for the continuation of rifting in the Sulu Sea inland, dated to around ∼9 Ma [Figure S1 43]. This inference is supported by crustal thickness measurements made across northern Borneo using the nBOSS dataset [30], which show a thinner crust (∼30 km), extending from the Sulu Sea towards central Sabah, coinciding with the exposed ophiolite complex. From these observations, it is also possible to conclude that the mean fast orientation across eastern Sabah is sub-parallel to the direction of the extension that would be expected due to rollback of the subducting Celebes Sea slab and opening of the Sulu Sea. In such extensional and/or rifting environments, stretching lineation, and hence ϕ, is expected to be parallel to the extension direction [36].

The lack of evidence for back-azimuthal variations in fast polarisations at KKM provides an additional line of evidence for horizontally layered anisotropy that is vertically coherent. It remains possible that there are multiple layers with similar orientations, though without earthquakes within this layer the vertical

integration of δt makes this indistinguishable from a single layer. Additionally, it only provides such a constraint for a small region around KKM, corresponding roughly with the width of the first Fresnel zone for the XKS phase arrivals. There may be multiple layers of anisotropy beyond this region that we are unable to identify due to the limited back-azimuthal coverage of our shear-wave splitting observations.

A small number of stations, located primarily to the south-east of Mount Kinabalu (see Figure 4), exhibit ϕ values that lie between the two dominant NE-SW and NW-SE trends. The surface geology in the region around Mount Kinabalu exhibits an exposed suite of peridotites, dated to ∼10 Ma—thus post-dating the formation of the Crocker Range. Geochemical analysis of zircons found within these peridotites points towards a subcontinental lithospheric mantle origin for these rocks, meaning they must have been uplifted and exposed within the last 10 Ma. A recent P-wave tomographic model for the mantle beneath Sabah has revealed a narrow, fast anomaly extending from the region of thinned lithosphere around the Semporna Peninsula (south-east Sabah), towards Mount Kinabalu, interpreted to represent a lithospheric drip that formed from the root of the Sulu Arc [30]. Thermo-mechanical modelling of a Rayleigh-Taylor gravitational instability, seeded by a small density perturbation representing the root of the volcanic arc, has been found to provide a reasonable explanation for the observed extension, and lithospheric thinning, around Mount Kinabalu [30]. Consequently, these observations may be an indication of a gradual overprinting of the orogen-parallel trend by localised extension related to the formation of a lithospheric instability from the root of the Sulu Arc. The relationship between events and processes in the tectonic history of the region and our observations is summarised in Figure 5.

Regional-scale tomographic models of Southeast Asia exhibit a high-velocity anomaly at between 200–300 km depth beneath northern Borneo [15], which is attributed to cold, subducted lithospheric material from either the Celebes Sea or the proto-South China Sea. Song et al. [40] attribute the fast orientation measured at KKM to LPO anisotropy induced by the deflection of mantle flow around the fossil slab segment of the proto-South China Sea subduction [inferred from tomographic studies, e.g. 15] or a thick lithospheric keel. Pilia et al. [30] have demonstrated the absence, however, of any strong anomaly in the mantle above 200 km that could potentially suggest that the imaged slab material has broken off and begun to sink into the lower mantle, the minimum depth of which is thought to be ∼250 km. Consequently, there is unlikely to be any remnant of 3-D mantle flow around the down-going slab or within the former mantle wedge, as is commonly seen in active subduction zones. For simple asthenospheric flow, the common mechanism by which strain is localised in the asthenosphere, the memory of this flow direction is thought to be only a few million years [35] based on the amount of strain required to completely reorient olivine aggregates

[27]. This interpretation also neglects the possible contribution due to fossil anisotropic fabric induced during the collision between the South China Sea continental margin and northern Borneo, which has since

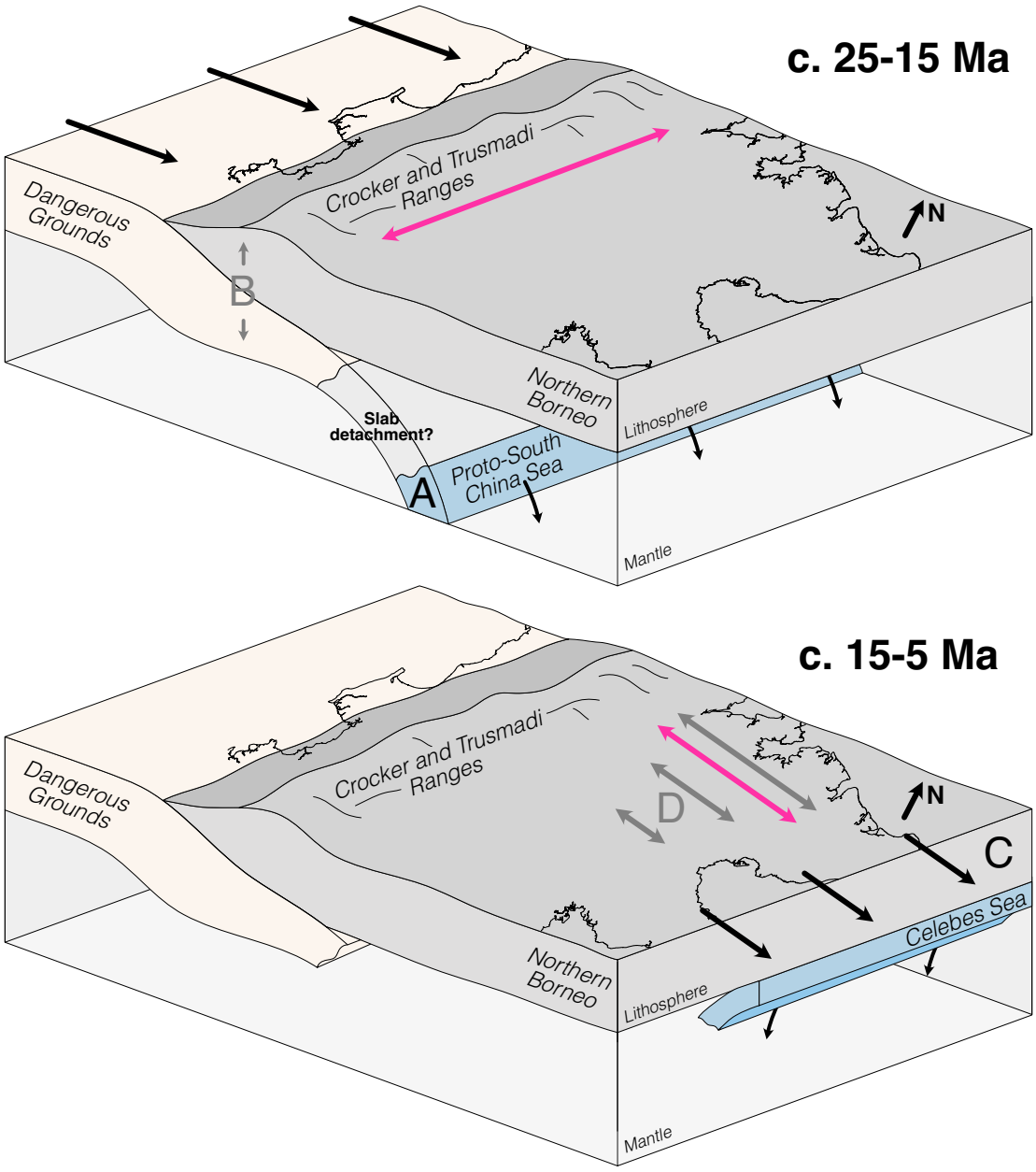

Figure 5: Summary cartoon showing the relationship between our observations of seismic anisotropy and events in the tectonic history of the region. The upper box model depicts the subduction of the proto-South China Sea (**A**), which was followed by continent-continent collision between the Dangerous Grounds and the north-western margin of northern Borneo. This collision led to the arcuate Rajang-Crocker orogeny and vertically coherent deformation in the resultant thickened crust and lithosphere (**B**). The lower box model depicts the subduction of the Celebes Sea and opening of the Sulu Sea via arc rollback (**C**), which may have promoted the propagation of extension into northern Borneo (**D**). Black arrows and letters denote directions of motion and the tectonic forces driving many of the observed tectonic phenomena, while grey arrows and letters denote responses to these forces and relate to the generation (and orientation) of the observed anisotropic fabrics (double-headed pink arrows).

been frozen into the lithosphere. There is a strong correlation between the lateral extent of this trend and the region showing a thickened lithosphere in Greenfield et al. [12], likely a result of the aforementioned continent-continent collision.

Without local, deep earthquakes beneath the study region, it is difficult to build any strong constraints on the depth distribution of seismic anisotropy. The short lengthscales ($\lesssim$ 40 km) over which there are observed changes in the fast orientation of anisotropy, however, does indicate that some degree of the observed shear-wave splitting is likely lithospheric in origin, so as to avoid a significant overlap in the first Fresnel zones of the phase arrivals at the network, which have a width of ∼150 km at the base of the lithosphere. Future work could make use of P-to-S conversions at significant boundaries, such as the Moho, or deep regional earthquakes from the Philippines and Sunda subduction zones (though the latter would primarily be useful for improving the azimuthal coverage, rather than the depth resolution).

4.1. Radial anisotropy

Radial anisotropy within the Earth can be constrained by the extraction of laterally averaged V_{S_V} and V_{S_H} from Rayleigh and Love wave phase velocities, where V_{S_V} and V_{S_H} are the wave speeds for vertically and horizontally polarised shear waves, respectively. The ratio of these two averaged velocities can be used as a measure of the degree of radial anisotropy as a function of depth, which can in turn be related to the tectonic processes that generate seismic anisotropy. In contrast to shear-wave splitting measurements, this technique has good vertical resolution, but at the cost of poorer lateral resolution. For A-type olivine fabric (the dominant fabric formed under standard mantle conditions), $V_{S_H}/V_{S_V} > 1$ (positive radial anisotropy) indicates horizontal flow or simple shear, and $V_{S_H}/V_{S_V} < 1$ (negative radial anisotropy) indicates vertical flow or pure shear shortening. Deformation by pure shear shortening may be an important factor in the generation of anisotropy in regions undergoing lithospheric shortening and thickening, proposed as an important stage in the generation of stable continental roots [31]. A key feature one would expect to see if there were significant anisotropy generated by simple asthenospheric flow is positive radial anisotropy below the lithosphere ($\gtrsim$100 km).

We extracted 1-D depth profiles of the radial anisotropy parameter, $\xi = (V_{S_H}/V_{S_V})^2$, from the *SASSY21* model, a recent 3-D full-waveform inversion tomographic model of Southeast Asia [46]. This model included waveform data down to a period of 20 s (slices through the ξ model are shown for various depths in supplementary Figure S10). Consequently, the velocities (and hence anisotropic structure) of the upper 50–100 km of the Earth are smoothed somewhat over this depth range, though the observed trend and sign in ξ remain valid. The averages of V_{S_H} and V_{S_V} were calculated at each depth slice within a small region

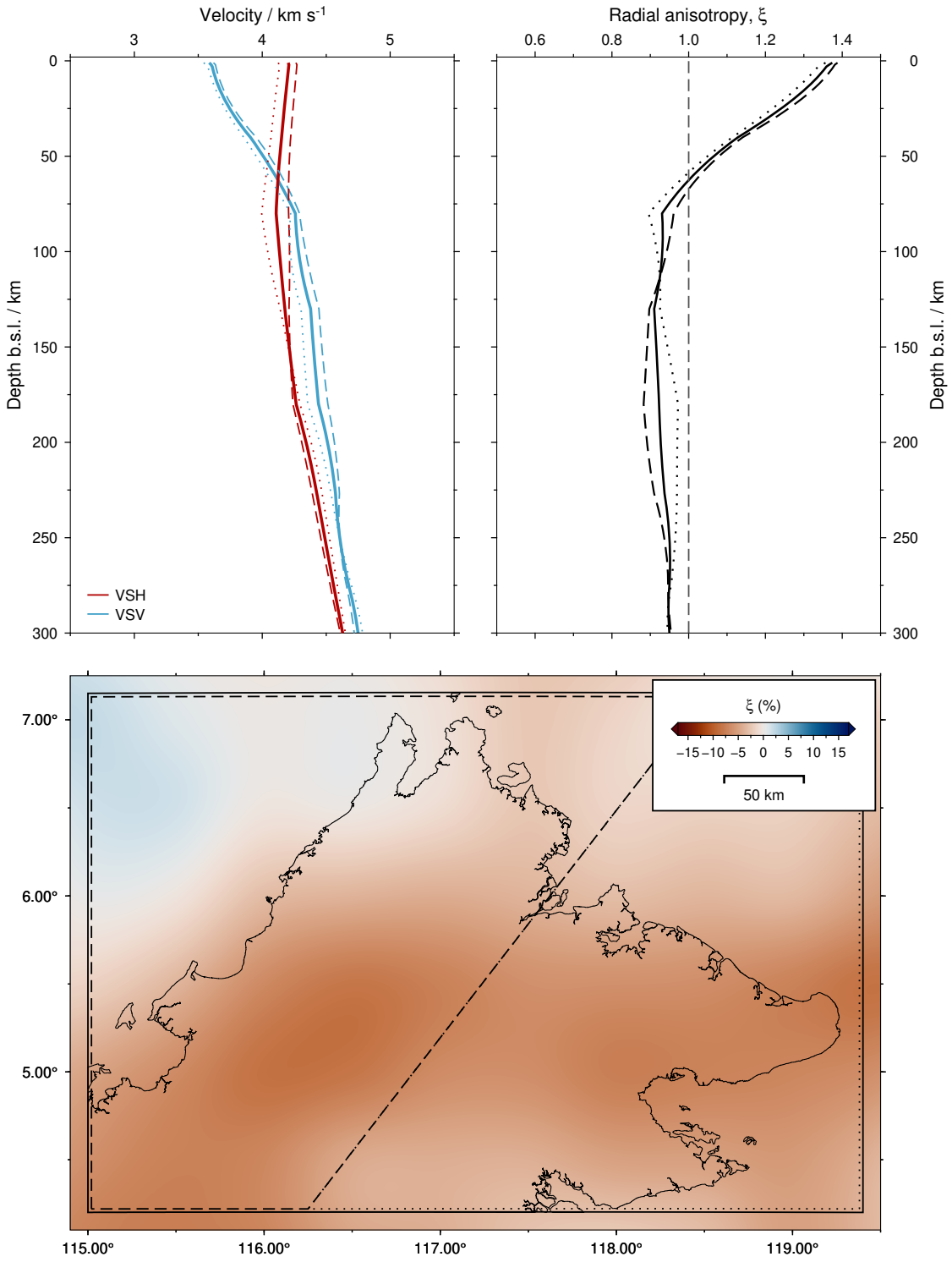

Figure 6: Depth profiles for V_{S_H} (red), V_{S_V} (blue), and ξ (black) extracted from the recent full-waveform tomographic model of Wehner et al. [46]. The solid lines correspond to the box encompassing the entirety of northern Borneo; the dashed lines correspond to the box encompassing trend 1 (north-west Sabah, striking ∼NE-SW); the dotted lines correspond to the box encompasing trend 2 (south-east Sabah, striking ∼NW-SE). The lower panel shows the geographic correspondence between the dashed/dotted/solid lines plotted on top of a horizontal slice through a radial anisotropy model derived from the full waveform inversion tomographic model, SASSY21, at 100 km depth [46].

of the model centred on northern Borneo, noting that *SASSY21* also exploited nBOSS waveform data, so there is good coverage in our study area. In addition, this region was subdivided into two sub-regions encompassing the two trends observed in the teleseismic shear-wave splitting dataset and 1-D profiles of the radial anisotropy were calculated (Figure 6).

The radial anisotropic structure of the upper 50–75 km appears to be positive ($\xi > 1$), indicating an anisotropic fabric with a primarily horizontal orientation that is consistent with LPO induced by both shortening and transpression at convergent boundaries (the orogen-parallel trend in the north-west of Sabah) and extension of continental material (Sulu Sea spreading trend in the south-east of Sabah). There is no indication of positive radial anisotropy at asthenospheric depths, which supports the conclusion that the observed seismic anisotropy is principally attributable to the lithosphere and corresponding mechanisms of deformation. There is some difference in the amplitude of negative radial anisotropy between 125–250 km depth, which may indicate some changes in the dynamic state of the mantle between these two regions, but this is beyond the scope of this study. The thickness of this observed layer is roughly consistent with the thickness of the lithosphere observed in Greenfield et al. [12].

5. Conclusions

We have investigated seismic anisotropy across northern Borneo using shear-wave splitting analysis of XKS phases recorded between March 2018 and January 2020. This has been supplemented by shear-wave splitting measurements at KKM, a permanent station operated by MetMalaysia, between January 2006 and January 2020. Across western Sabah, most notably beneath the Crocker Range, we find orogen parallel anisotropy striking at N063°E ± 14°, likely reflecting 'fossil' anisotropy in the lithosphere formed during the collision of the continental Dangerous Grounds with the continental margin of northern Sabah. Indeed, the observed delay times of 0.6–1.8 s are consistent with a 60–180 km thick layer with 4% anisotropy (or, conversely, a 100 km thick layer with 2.4–7.2% anisotropy). Our observations do not definitively constrain whether the anisotropy beneath northern Borneo is simple or complex (for example due to multiple or dipping layers), though we do show that a simple model is sufficient to explain our observations. This may indicate that the sub-lithospheric mantle is either isotropic, weakly anisotropic, or possesses the same anisotropic fabric as the lithosphere, but further analysis, particularly incorporating information derived from surface waves, would be beneficial. In eastern Sabah, the orientation of anisotropy is nearly orthogonal to the trend observed in the west and is sub-parallel to both the absolute plate motion and the direction of spreading of the Sulu Sea, striking at N112°E ± 19°. This trend extends inland to central Sabah, where

it terminates, correlating well with the extent of onshore spreading inferred from recent U-Pb dating. The rapid transition between these two dominant trends (over $\lesssim$ 40 km) suggests that the anisotropic source is shallow. A reduction in the observed delay times seen in south-central Sabah, including a number of null stations, may indicate the presence of vertical mantle flow, such as that induced by a lithospheric drip. A number of stations in the vicinity of Mount Kinabalu exhibit fast orientations that lie between the two main trends, possibly indicating the gradual overprinting of the fossil fabric in response to localised extension and thinning of the lithosphere. These results constitute strong evidence for a system of mechanisms focussed predominantly within the lithosphere as the primary controls on seismic anisotropy in this post-subduction continental setting, with little influence from present-day mantle flow.

6. Acknowledgements

The authors thank all those that contributed to the deployment, servicing, and recovery of the northern Borneo Orogeny Seismic Survey (nBOSS) network between March 2018 and January 2020. We also thank Miriam Reiss for assistance with SplitRacer (which can be downloaded from https://www.geophysik.uni-frankfurt.de/64002762/Software) and helpful discussions of the results presented herein. We have made extensive use of Python for our analysis, including the open-source packages: NumPy (1.21.5), SciPy (1.8.0), pandas (1.4.1), Matplotlib (3.5.1), and ObsPy (1.2.2). A number of figures were produced using the Generic Mapping Tools (6.3.0). S.P. acknowledges support from the Natural Environmental Research Council (NERC) Grant NE/R013500/1 and from the European Union's Horizon 2020 Research and Innovation Program under Marie Skłodowska-Curie Grant Agreement 790203. Seismometers used in the nBOSS network were provided by the Universities of Cambridge and Aberdeen, and the Natural Environment Research Council (NERC) Geophysical Equipment Facility (loan 1038). Waveform data recorded by the nBOSS network were extracted, quality checked, and archived by C. A. Bacon. We thank MetMalaysia for providing access to their restricted continuous waveform data recorded by their permanent MY network in Sabah. Seismic data from the nBOSS network will be accessible through the IRIS Data Management Center (https://ds.iris.edu/ds/nodes/dmc/) from February 2023 (see doi: 10.7914/SN/YC_2018). Supplementary datafiles, including cut and bandpass filtered waveforms, can be downloaded from doi: 10.5281/zenodo.6461787. Code for performing the multi-layer anisotropy modelling is available from doi: 10.5281/zenodo.5931586. All code required to reproduce the visualisations presented in this study can be downloaded from doi: 10.5281/zenodo.6480581. Department of Earth Sciences, Cambridge contribution ESC.XXXX.

References

[1] Argus, D. F., Gordon, R. G., & Demets, C. (2011). Geologically current motion of 56 plates relative to the no-net-rotation reference frame. *Geochemistry, Geophysics, Geosystems*, *12*, 1–13. doi:10.1029/2011GC003751.

[2] Bowman, J. R., & Ando, M. (1987). Shear-wave splitting in the upper-mantle wedge above the Tonga subduction zone. *Geophysical Journal of the Royal Astronomical Society*, *88*, 25–41. doi:10.1111/j.1365-246X.1987.tb01367.x.

[3] Cao, L., He, X., Zhao, L., ChuanChuan, L., Hao, T., Zhao, M., & Qiu, X. (2021). Mantle Flow Patterns Beneath the Junction of Multiple Subduction Systems Between the Pacific and Tethys Domains, SE Asia: Constraints From SKS-Wave Splitting Measurements. *Geochemistry, Geophysics, Geosystems*, *22*, 1–17. doi:10.1029/2021GC009700.

[4] Chevrot, S. (2000). Multichannel analysis of shear wave splitting. *Journal of Geophysical Research*, *105*, 21579–21590. doi:10.1029/2000JB900199.

[5] Cottam, M. A., Hall, R., Sperber, C., Kohn, B. P., Forster, M. A., & Batt, G. E. (2013). Neogene rock uplift and erosion in northern Borneo: Evidence from the Kinabalu granite, Mount Kinabalu. *Journal of the Geological Society*, *170*, 805–816. doi:10.1144/jgs2011-130.

[6] Debayle, E., & Ricard, Y. (2013). Seismic observations of large-scale deformation at the bottom of fast-moving plates. *Earth and Planetary Science Letters*, *376*, 165–177. doi:10.1016/j.epsl.2013.06.025.

[7] Eakin, C. M., Long, M. D., Wagner, L. S., Beck, S. L., & Tavera, H. (2015). Upper mantle anisotropy beneath Peru from SKS splitting: Constraints on flat slab dynamics and interaction with the Nazca Ridge. *Earth and Planetary Science Letters*, *412*, 152–162. doi:10.1016/j.epsl.2014.12.015.

[8] Eakin, C. M., Rychert, C. A., & Harmon, N. (2018). The Role of Oceanic Transform Faults in Seafloor Spreading: A Global Perspective From Seismic Anisotropy. *Journal of Geophysical Research: Solid Earth*, *123*, 1736–1751. doi:10.1002/2017JB015176.

[9] Fischer, K. M., Parmentier, E. M., Stine, A. R., & Wolf, E. R. (2000). Modeling anisotropy and plate-driven flow in the Tonga subduction zone back arc. *Journal of Geophysical Research: Solid Earth*, *105*, 16181–16191. doi:10.1029/1999jb900441.

[10] Fry, B., Deschamps, F., Kissling, E., Stehly, L., & Giardini, D. (2010). Layered azimuthal anisotropy of Rayleigh wave phase velocities in the European Alpine lithosphere inferred from ambient noise. *Earth and Planetary Science Letters*, *297*, 95–102. doi:10.1016/j.epsl.2010.06.008.

[11] Gilligan, A., Bastow, I. D., Watson, E., Darbyshire, F. A., Levin, V., Menke, W., Lane, V., Hawthorn, D., Boyce, A., Liddell, M. V., & Petrescu, L. (2016). Lithospheric deformation in the Canadian appalachians: Evidence from shear wave splitting. *Geophysical Journal International*, *206*, 1273–1280. doi:10.1093/gji/ggw207.

[12] Greenfield, T., Gilligan, A., Pilia, S., Cornwell, D. G., Tongkul, F., Widiyantoro, S., & Rawlinson, N. (2022). Post-subduction tectonics of Sabah, northern Borneo, inferred from surface wave tomography. *Geophysical Research Letters*, *49*, e2021GL096117. doi:10.1029/2021GL096117.

[13] Hall, R. (1996). Reconstructing Cenozoic SE Asia. *Tectonic Evolution of Southeast Asia*, (pp. 153–184).

[14] Hall, R. (2013). Contraction and extension in northern Borneo driven by subduction rollback. *Journal of Asian Earth Sciences*, *76*, 399–411. doi:10.1016/j.jseaes.2013.04.010.

[15] Hall, R., & Spakman, W. (2015). Mantle structure and tectonic history of SE Asia. *Tectonophysics*, *658*, 14–45. doi:10.1016/j.tecto.2015.07.003.

[16] Hutchison, C. S., Bergman, S. C., Swauger, D. A., & Graves, J. E. (2000). A Miocene collisional belt in north Borneo: uplift

mechanism and isostatic adjustment quantified by thermochronology. *Journal of the Geological Society*, *157*, 783–793. doi:10.1144/jgs.157.4.783.

[17] Jung, H., Katayama, I., Jiang, Z., Hiraga, T., & Karato, S. (2006). Effect of water and stress on the lattice-preferred orientation of olivine. *Tectonophysics*, *421*, 1–22. doi:10.1016/j.tecto.2006.02.011.

[18] Karato, S.-I. (1995). Effects of water on seismic wave velocities in the upper mantle. *Proceedings of the Japan Academy, Series B*, *71*, 61–66. doi:10.2183/pjab.71.61.

[19] Kaviani, A., Mahmoodabadi, M., Rümpker, G., Pilia, S., Tatar, M., Nilfouroushan, F., Yamini-Fard, F., Moradi, A., & Ali, M. Y. (2021). Mantle-flow diversion beneath the Iranian plateau induced by Zagros' lithospheric keel. *Scientific Reports*, *11*, 1–12. doi:10.1038/s41598-021-81541-9.

[20] Kennett, B. L., Engdahl, E. R., & Buland, R. (1995). Constraints on seismic velocities in the Earth from traveltimes. *Geophysical Journal International*, *122*, 108–124. doi:10.1111/j.1365-246X.1995.tb03540.x.

[21] Lai, C. K., Xia, X. P., Hall, R., Meffre, S., Tsikouras, B., Rosana Balangue-Tarriela, M. I., Idrus, A., Ifandi, E., & aqidah Norazme, N. (2021). Cenozoic Evolution of the Sulu Sea Arc-Basin System: An Overview. *Tectonics*, *40*, 1–26. doi:10.1029/2020TC006630.

[22] Liddell, M. V., Bastow, I., Darbyshire, F., Gilligan, A., & Pugh, S. (2017). The formation of Laurentia: Evidence from shear wave splitting. *Earth and Planetary Science Letters*, *479*, 170–178. doi:10.1016/j.epsl.2017.09.030.

[23] Macpherson, C. G., Chiang, K. K., Hall, R., Nowell, G. M., Castillo, P. R., & Thirlwall, M. F. (2010). Plio-Pleistocene intra-plate magmatism from the southern Sulu Arc, Semporna peninsula, Sabah, Borneo: Implications for high-Nb basalt in subduction zones. *Journal of Volcanology and Geothermal Research*, *190*, 25–38. doi:10.1016/j.jvolgeores.2009.11.004.

[24] Merry, T. A., Bastow, I. D., Kounoudis, R., Ogden, C. S., Bell, R. E., & Jones, L. (2021). The Influence of the North Anatolian Fault and a Fragmenting Slab Architecture on Upper Mantle Seismic Anisotropy in the Eastern Mediterranean. *Geochemistry, Geophysics, Geosystems*, *22*, 1–26. doi:10.1029/2021GC009896.

[25] Morley, C. K., & Back, S. (2008). Estimating hinterland exhumation from late orogenic basin volume, NW Borneo. *Journal of the Geological Society*, *165*, 353–366. doi:10.1144/0016-76492007-067.

[26] Nicolas, A. (1993). Why fast polarization directions of SKS seismic waves are parallel to mountain belts. *Physics of the Earth and Planetary Interiors*, *78*, 337–342. doi:10.1016/0031-9201(93)90164-5.

[27] Nicolas, A., Boudier, F., & Boullier, A. (1973). Mechanisms of flow in naturally and experimentally deformed peridotites. *American Journal of Science*, *273*, 853–876.

[28] Nicolas, A., & Christensen, N. I. (1987). Formation of anisotropy in upper mantle peridotites—A review. *Composition, Structure and Dynamics of the Lithosphere-Asthenosphere System*, *16*, 111–123. doi:10.1029/GD016p0111.

[29] Pilia, S., Arroucau, P., Rawlinson, N., Reading, A., & Cayley, R. (2016). Inherited crustal deformation along the East Gondwana margin revealed by seismic anisotropy tomography. *Geophysical Research Letters*, *43*, 12–082. doi:10.1002/2016GL071201.

[30] Pilia, S., Davies, D., Hall, R., Bacon, C., Gilligan, A., Greenfield, T., Tongkul, F., Kramer, S., Cornwell, D., Colli, L., & Rawlinson, N. (2021). Effects of post-subduction processes on continental lithosphere, . doi:10.21203/rs.3.rs-861968/v1.

[31] Priestley, K., Ho, T., & McKenzie, D. (2021). The formation of continental roots. *Geology*, *49*, 190–194. doi:10.1130/G47696.1.

[32] Reiss, M. C., & Rümpker, G. (2017). SplitRacer: MATLAB code and GUI for semiautomated analysis and interpretation of teleseismic shear-wave splitting. *Seismological Research Letters*, *88*, 392–409. doi:10.1785/0220160191.

[33] Russo, R. M., & Silver, P. G. (1994). Trench-parallel flow beneath the Nazca plate from seismic anisotropy. *Science*, *263*, 1105–1111. doi:10.1126/science.263.5150.1105.

[34] Savage, M. K. (1999). Seismic anisotropy and mantle deformation: What have we learned from shear wave splitting? *Reviews of Geophysics*, *37*, 65–106. doi:10.1029/98RG02075.

[35] Silver, P., Mainprice, D., Ismaïl, W. B., Tommasi, A., & Barruol, G. (1999). Mantle structural geology from seismic anisotropy. *Mantle Petrology: Field Observations and High Pressure Experimentations*, (pp. 79–103).

[36] Silver, P. G. (1996). Seismic anisotropy beneath the continents: Probing the depths of geology. *Annual Review of Earth and Planetary Sciences*, *24*, 385–432. doi:10.1146/annurev.earth.24.1.385.

[37] Silver, P. G., & Chan, W. W. (1988). Implications for continental structure and evolution from seismic anisotropy. *Nature*, *335*, 34–39. doi:10.1038/335034a0.

[38] Silver, P. G., & Chan, W. W. (1991). Shear wave splitting and subcontinental mantle deformation. *Journal of Geophysical Research*, *96*, 16429–16454. doi:10.1029/91jb00899.

[39] Silver, P. G., & Savage, M. K. (1994). The interpretation of shear-wave splitting parameters in the presence of two anisotropy layers. *Geophysical Journal International*, *119*, 949–963. doi:10.1111/j.1365-246X.1994.tb04027.x.

[40] Song, W., Yu, Y., Gao, S. S., Liu, K. H., & Fu, Y. (2021). Seismic Anisotropy and Mantle Deformation Beneath the Central Sunda Plate. *Journal of Geophysical Research: Solid Earth*, *126*. doi:10.1029/2020JB021259.

[41] Tongkul, F. (1991). Tectonic evolution of Sabah, Malaysia. *Journal of Southeast Asian Earth Sciences*, *6*, 395–405. doi:10.1016/0743-9547(91)90084-B.

[42] Tongkul, F. (1993). Tectonic control on the development of the Neogene basins in Sabah, East Malaysia. *Bulletin of the Geological Society of Malaysia*, *33*, 95–103.

[43] Tsikouras, B., La, C. K., Ifandi, E., Norazme, N. A., Teo, C. H., & Xia, X. P. (2021). New zircon radiometric U-Pb ages and Lu-Hf isotopic data from the ultramafic-mafic sequences Of Ranau And Telupid (Sabah, Eastern Malaysia): time to reconsider the geological evolution of Southeast Asia? *Geology*, *49*, 789–793. doi:10.1130/G48126.1.

[44] Vinnik, L. P., Farra, V., & Romanowicz, B. (1989). Azimuthal anisotropy in the Earth from observations of SKS at GEOSCOPE and NARS broadband stations. *Bulletin of the Seismological Society of America*, *79*, 1542–1558.

[45] Walsh, E., Arnold, R., & Savage, M. K. (2013). Silver and Chan revisited. *Journal of Geophysical Research: Solid Earth*, *118*, 5500–5515. doi:10.1002/jgrb.50386.

[46] Wehner, D., Blom, N., Rawlinson, N., Daryono, Böhm, C., Miller, M. S., Supendi, P., & Widiyantoro, S. (2021). SASSY21: A 3-D seismic structural model of the lithosphere and underlying mantle beneath Southeast Asia from multi-scale adjoint waveform tomography. *Journal of Geophysical Research: Solid Earth*, (p. e2021JB022930).

[47] West, J. D., Fouch, M. J., Roth, J. B., & Elkins-Tanton, L. T. (2009). Vertical mantle flow associated with a lithospheric drip beneath the Great Basin. *Nature Geoscience*, *2*, 439–444. doi:10.1038/ngeo526.

[48] Wolfe, C. J., & Silver, P. G. (1998). Seismic anisotropy of oceanic upper mantle: Shear wave splitting methodologies and observations. *Journal of Geophysical Research: Solid Earth*, *103*, 749–771. doi:10.1029/97jb02023.

[49] Xue, M., Le, K. P., & Yang, T. (2013). Seismic anisotropy surrounding South China Sea and its geodynamic implications. *Marine Geophysical Research*, *34*, 407–429. doi:10.1007/s11001-013-9194-4.

[50] Zhang, Z., & Karato, S. (1995). Lattice preferred orientation of olivine aggregates in simple shear. *Nature*, *375*, 774–777. doi:10.1038/375774a0.

Supplementary information to the manuscript

The signature of lithospheric anisotropy at post-subduction continental margins: new insight from XKS splitting analysis in northern Borneo

Conor A. Bacon[a,*], Nick Rawlinson[a], Simone Pilia[a,b], Amy Gilligan[c], Deborah Wehner[a], David G. Cornwell[c], Felix Tongkul[d]

*Corresponding author, conor.bacon@cantab.net

This file contains additional text, figures, and data tables to supplement the above manuscript.

Supplementary figure summary
Figure S1: Geological map of Sabah

Figure S2: Labelled network map

Figure S3: Earthquake catalogue overview

Figure S4: Example of a good shear-wave splitting measurement

Figure S5: Example of a null shear-wave splitting measurement

Figure S6: n-layer modelling at KKM

Figure S7: Shear-wave splitting results plotted on top of crustal thickness estimates from VDSS

Figure S8: Shear-wave splitting results plotted on top of crustal thickness estimates from joint inversion of receiver functions and surface waves

Figure S9: Shear-wave splitting results plotted on top of horizontal slice through FWI tomographic model at 100 km depth

Figure S10: Slices through FWI tomographic model at a range of depths across the entire region of Southeast Asia

Supplementary files summary
Supplementary file 1: nBOSS network instrument locations

Supplementary file 2: MetMalaysia network instrument locations

Supplementary file 3: Earthquake catalogue for 2018-2020

Supplementary file 4: Earthquake catalogue for 2006-2020

Supplementary file 5: Regions use for calculating radial anisotropy from FWI tomography model

Supplementary file 6: All shear-wave splitting measurements, including grades

Supplementary file 7: 1-layer average shear-wave splitting results

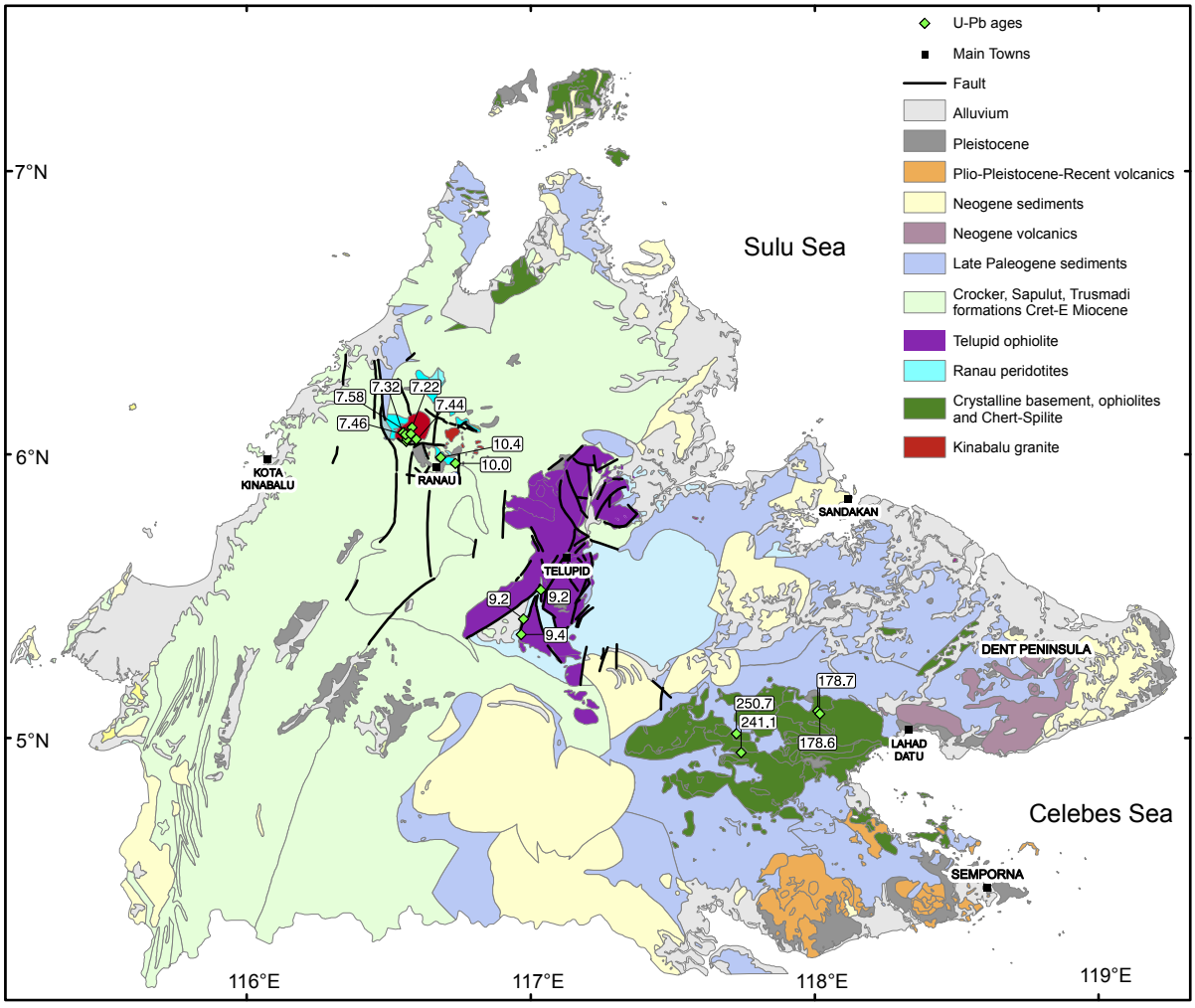

Figure S1: Simplified surface geology map of Sabah, adapted from Pilia et al. (2021). Geochemical dating from Lai et al., 2021.

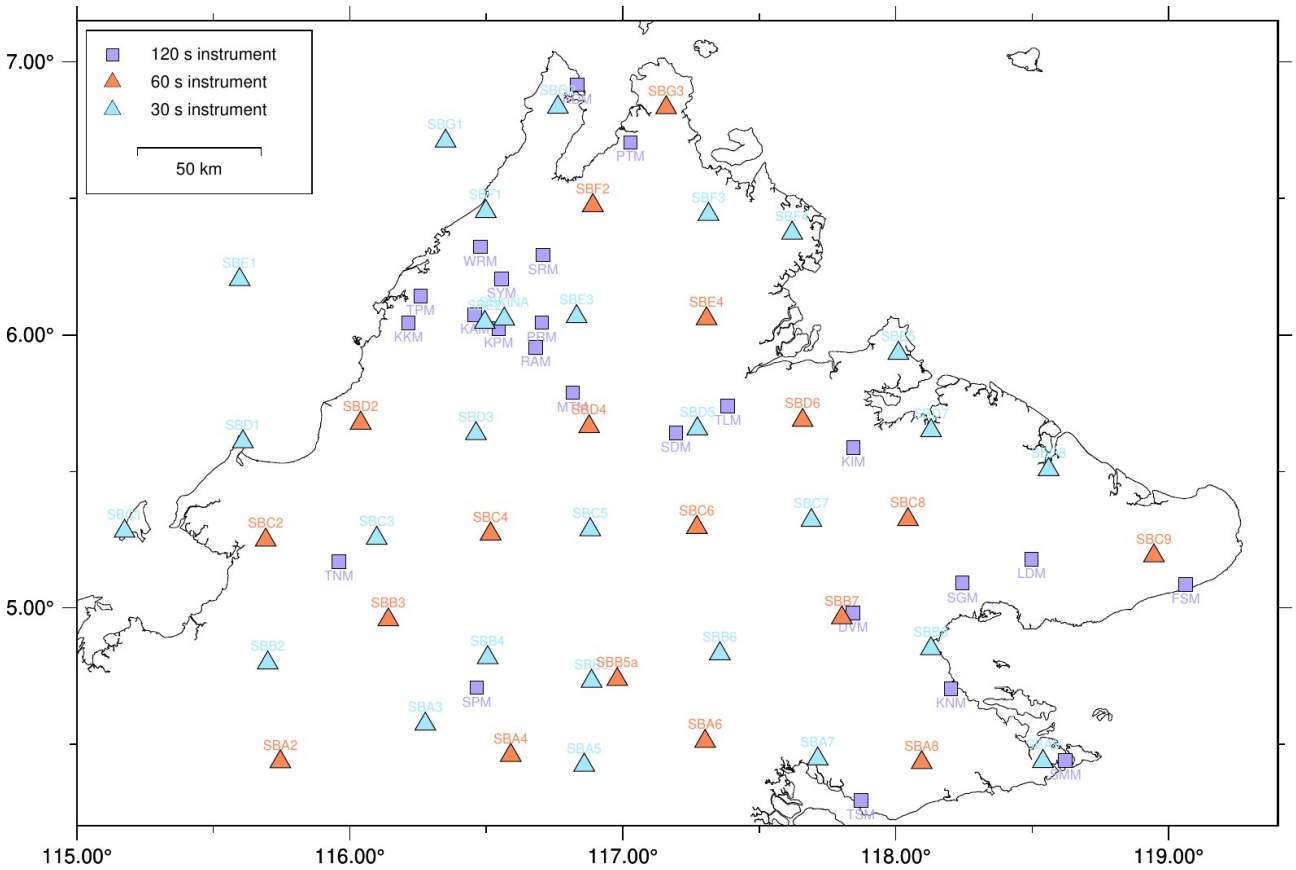

Figure S2: Map showing networks used in this study, including all station names. Stations in the nBOSS network are denoted by triangles, while stations in the permanent MetMalaysia network are denoted by squares.

Figure S3: Source maps, shown using a polar projection centred on northern Borneo, for this study. Panels a and b show the events in the periods 2018–2020 and 2006–2020, respectively. The azimuthal coverage is represented by the coloured 5° segments, with red shading indicating no events in the segment. As expected, there is far greater coverage as a function of back azimuth for the longer period study at the permanent station KKM.

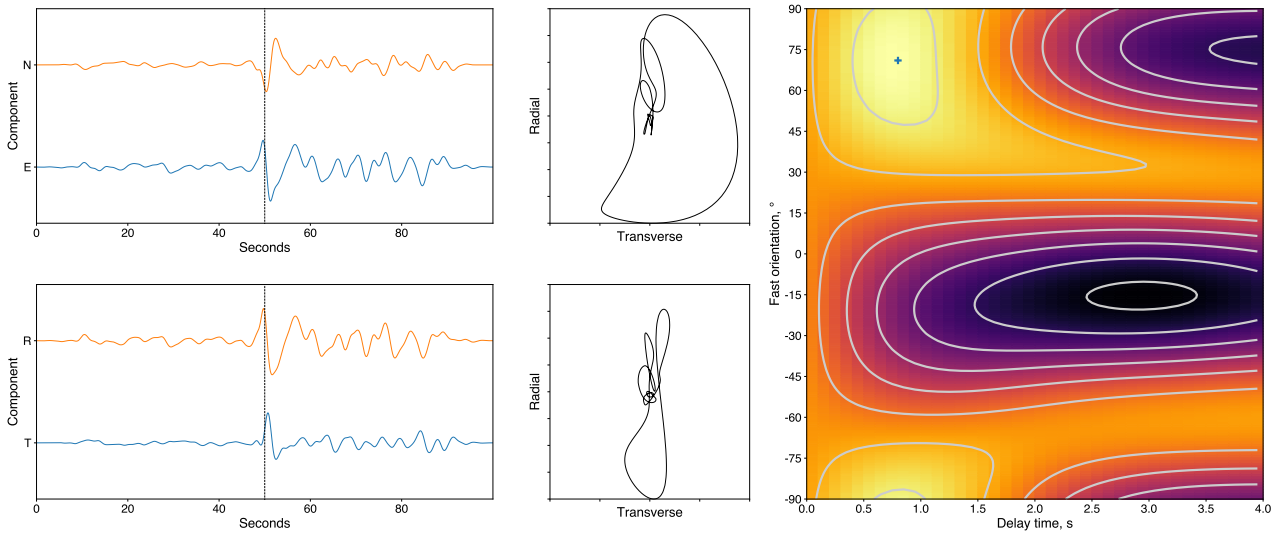

Figure S4: An example of a good measurement of an SKS phase arrival at SBC8. Panel **a** shows the uncorrected north and east component data. Panel **b** shows the uncorrected data rotated onto the radial and transverse components. Panels **c** and **d** show the particle motions for the uncorrected and corrected waveform data, respectively. There is no evidence of elliptical particle motion in the uncorrected data, a key indicator of a null measurement. Panel **e** shows the resultant energy grid from the splitting analysis.

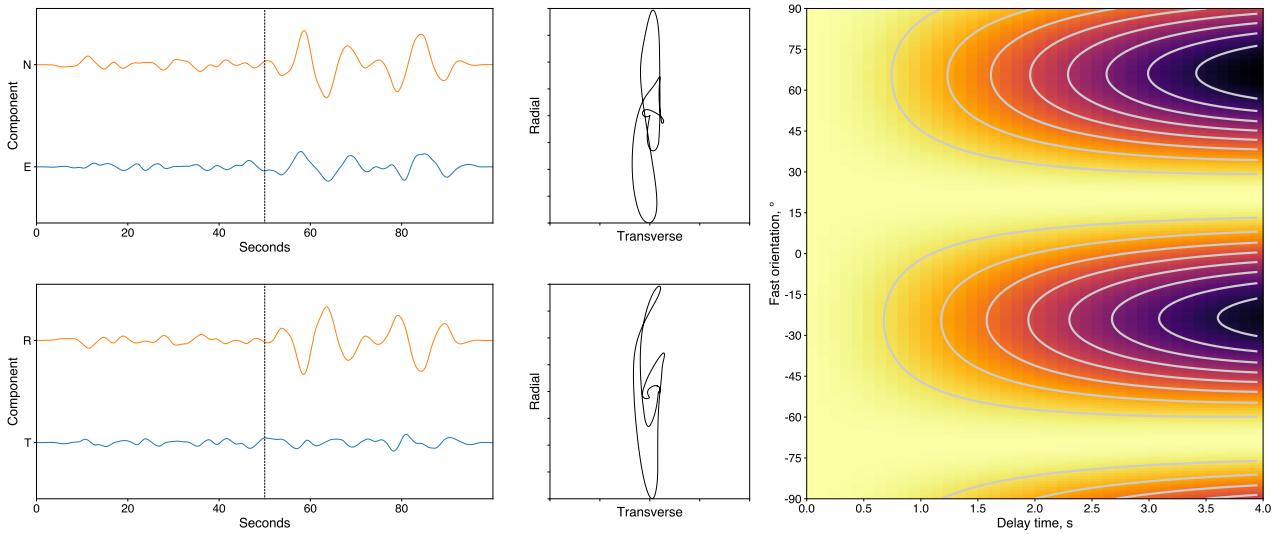

Figure S5: An example of a null measurement of an SKS phase arrival at SBA8. The panels are the same as in Figure 9.3. There is no evidence of elliptical particle motion in the uncorrected data, a key indicator of a null measurement. The resultant energy grid from the splitting analysis shows the characteristic null pattern.

We use the open-source toolkit AnisotroPy (Bacon, 2022; doi: 10.5281/zenodo.5931586) to model back-azimuthal variations in splitting parameters that may be caused by multiple anisotropic layers (Silver & Savage, 1994), employing the same misfit-minimisation approach set out by Liddell et al. (2017), to explore whether the results at the permanent MetMalaysia station, KKM, can be reasonably explained by 1-, 2-, or dipping-layers of anisotropy. The approach is outlined in the supplementary information to Merry et al. (2021). For each observed pair of splitting parameters, we calculate the misfit,

$$\Gamma_p(x) = |(p_{obs} - p_{mod}(x))| - \Delta_p,$$

where x is the assumed azimuth of the incoming wave, which we vary from 5° less than to 5° greater than the calculated azimuth of the observed shear wave; $p_{mod}(x)$ is the predicted splitting parameter from the model being tested; and Δ_p is the calculated error in the splitting parameter. If the difference between model and observation is less than σ, we set $\Gamma = 0$. Taking the minimum value of $\Gamma_p(x)$ for each pair of splitting parameters, we then calculate the root mean square misfit (RMS) across all observations for the given model ($RMS_p = \sqrt{\Sigma(\Gamma_p)^2 / n_p}$). To calculate an overall misfit to characterise a model, we normalised RMS_φ and $RMS_{\delta t}$ by the standard deviation (σ) in the observed splitting parameters, i.e.

$$M = \frac{RMS_\phi}{\sigma_\phi} + \frac{RMS_{\delta t}}{\sigma_{\delta t}}$$

The inputs for the two-layer model are anisotropic strength, layer thickness, T, and fast direction azimuth, φ. Layer thickness and anisotropic strength directly trade off, so we assume an anisotropic strength of 4% (Savage, 1999), and perform grid searches across T and φ to minimise the value of M, as defined above. All effective splitting parameters are evaluated for an angle of incidence of 11.2262°, which corresponds to the typical incidence angle of an SKS phase. We find a minimum for a 2-layer model consisting of a lower layer with a thickness of 25 km and fast direction of -12° and an upper layer with a thickness of 150 km and fast direction of 58°. This has a final misfit value of M = 8.98. A single layer with a thickness of 110 km and fast direction orientation of 68° (as would fit the parameters returned by the joint splitting analysis at KKM) has a final misfit value of M = 8.91. Consequently, we deem these measures of the fit of the given models to the observations do not provide sufficient evidence in favour of one model over another and, at best, favour a single layer model.

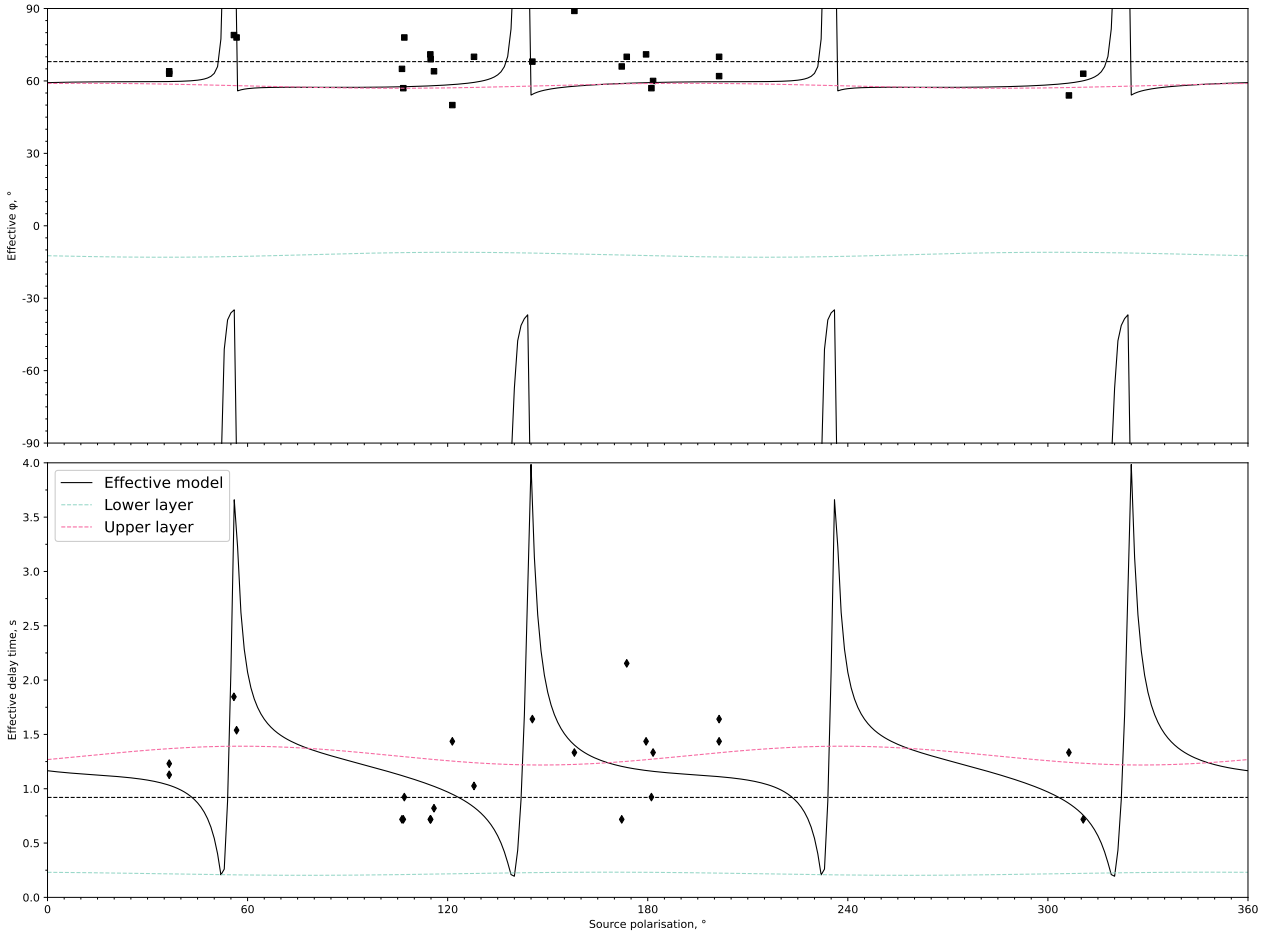

Figure S6: n-layer modelling for results at KKM, showing it is difficult to distinguish between the best-fitting 2-layer model (with the upper and lower layers show by the blue and pink dashed lines, respectively). The solid black lines shows the effective splitting, per the equations set out in Silver and Savage, 1994. The dashed black lines show the best-fitting single layer model recovered from joint inversion of the shear-wave splitting observations.

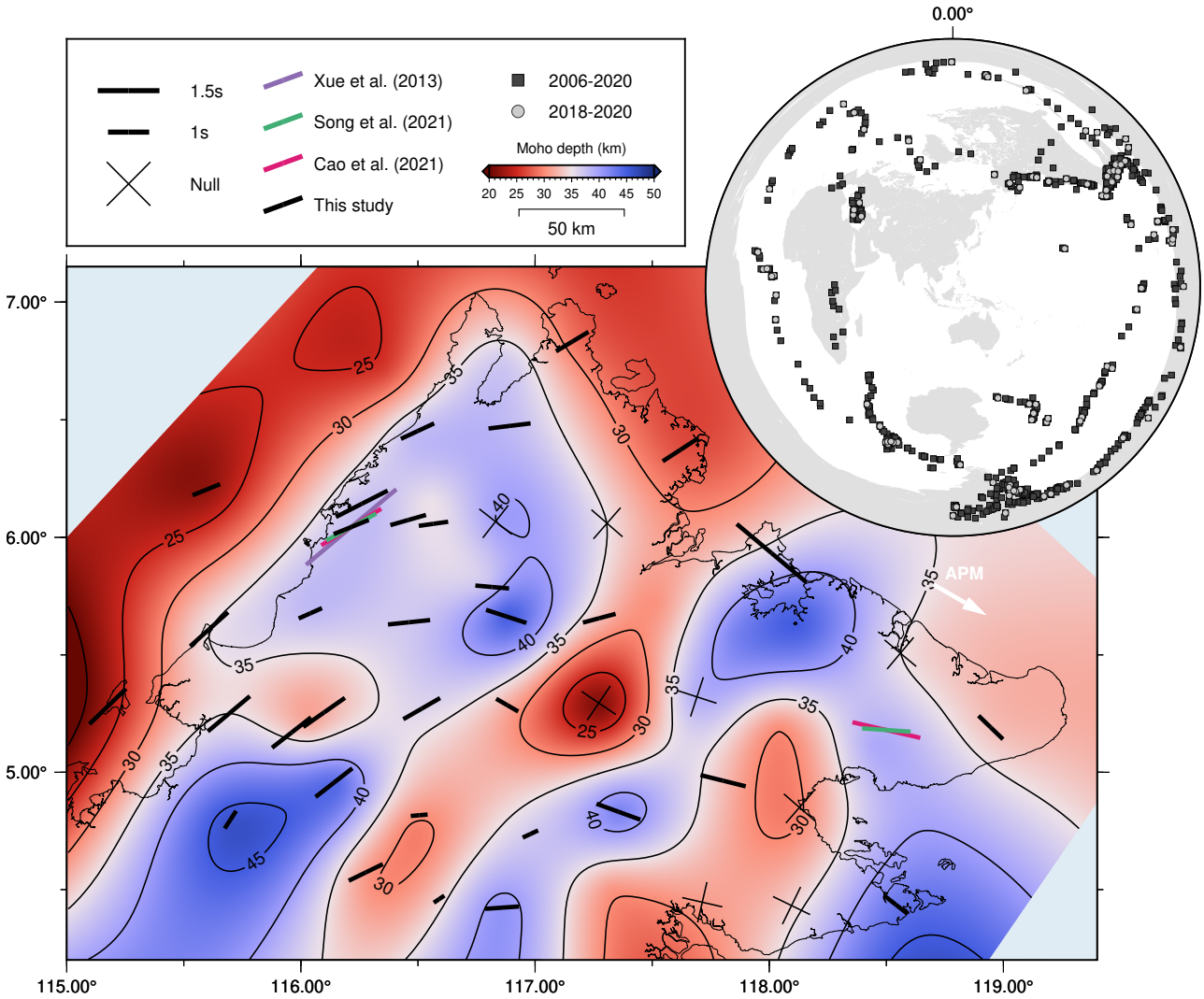

Figure S7: Map of station-averaged XKS splitting measurements from this study (black) and the studies of Xue et al. (2013) (purple), Song et al. (2021) (green), and Cao et al. (2021) (magenta). The white arrow represents the current Absolute Plate Motion which has a bearing of N120°E according to the NNR-MORVEL56 plate model (Argus et al. 2011). These results are shown on top of the Moho boundary depth (i.e. the crustal thickness) as determined from Virtual Deep Seismic Sounding (Linang et al., 2022).

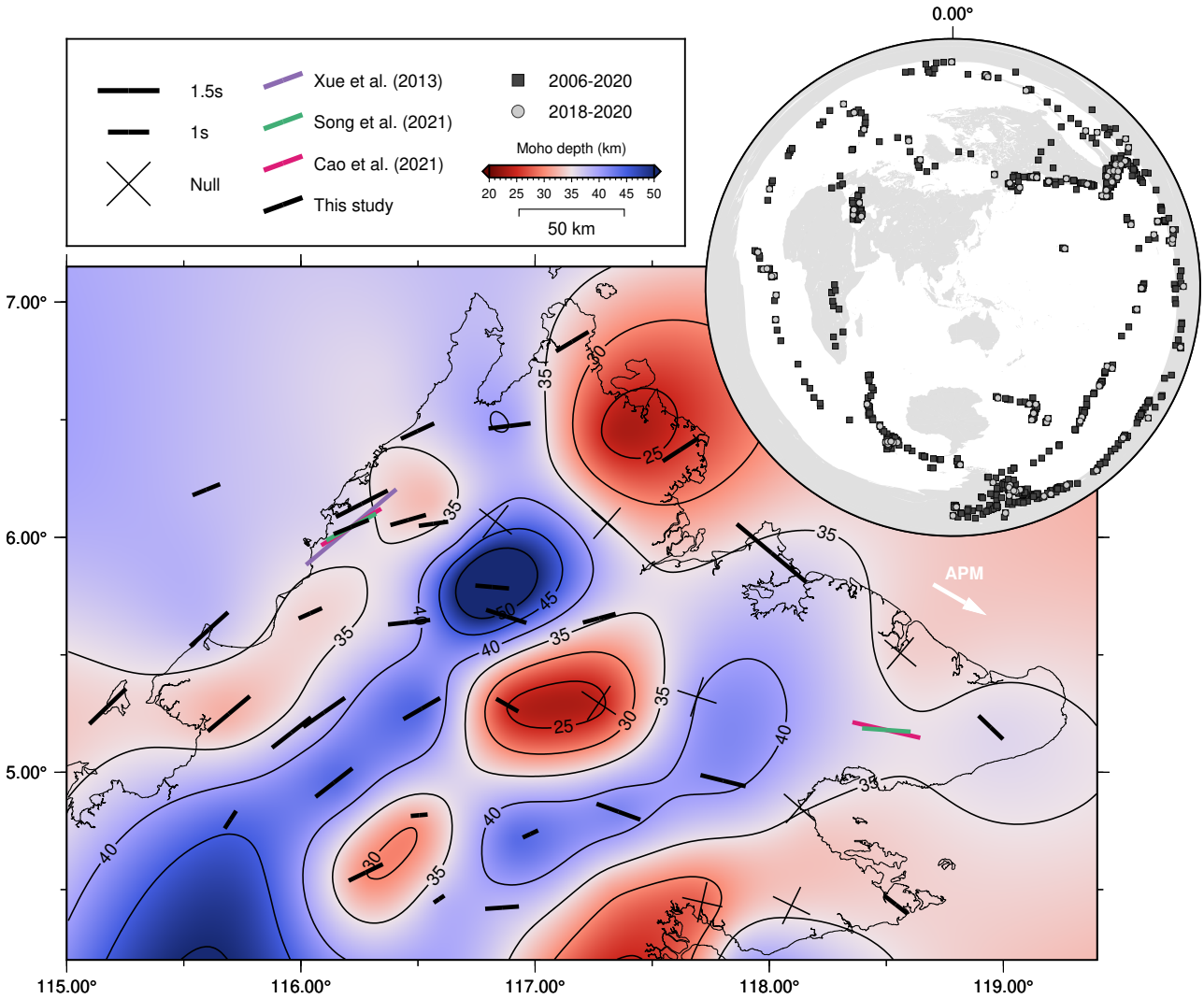

Figure S8: Map of station-averaged XKS splitting measurements from this study (black) and the studies of Xue et al. (2013) (purple), Song et al. (2021) (green), and Cao et al. (2021) (magenta). The white arrow represents the current Absolute Plate Motion which has a bearing of N120°E according to the NNR-MORVEL56 plate model (Argus et al. 2011). These results are shown on top of the Moho boundary depth (i.e. the crustal thickness) as determined from receiver function analysis (Pilia et al., 2021).

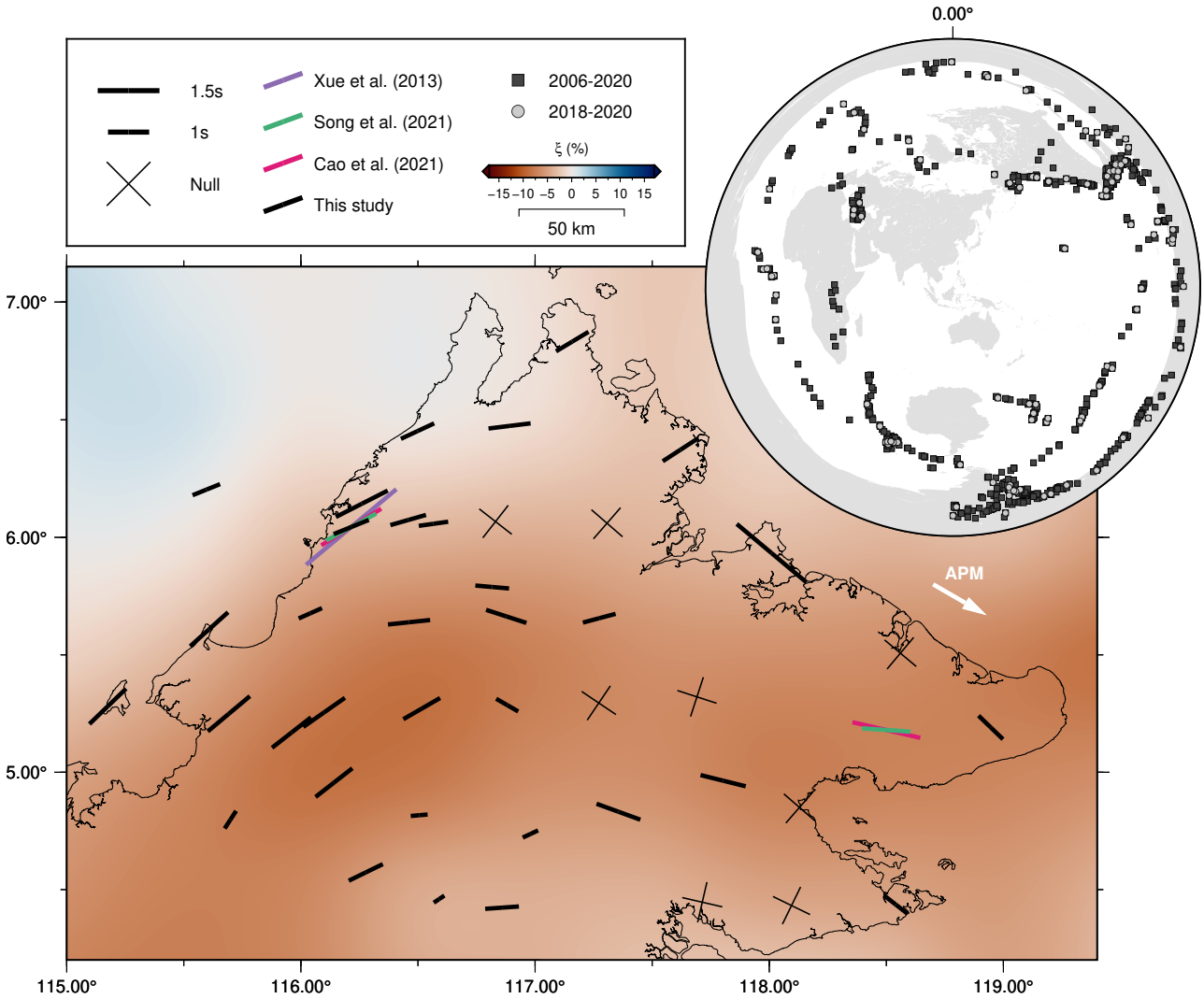

Figure S9: Map of station-averaged XKS splitting measurements from this study (black) and the studies of Xue et al. (2013) (purple), Song et al. (2021) (green), and Cao et al. (2021) (magenta). The white arrow represents the current Absolute Plate Motion which has a bearing of N120°E according to the NNR-MORVEL56 plate model (Argus et al. 2011). These results are shown on top of a horizontal slice through a radial anisotropy model derived from the full waveform inversion tomographic model, SASSY21, at 100 km depth (Wehner et al., 2022).

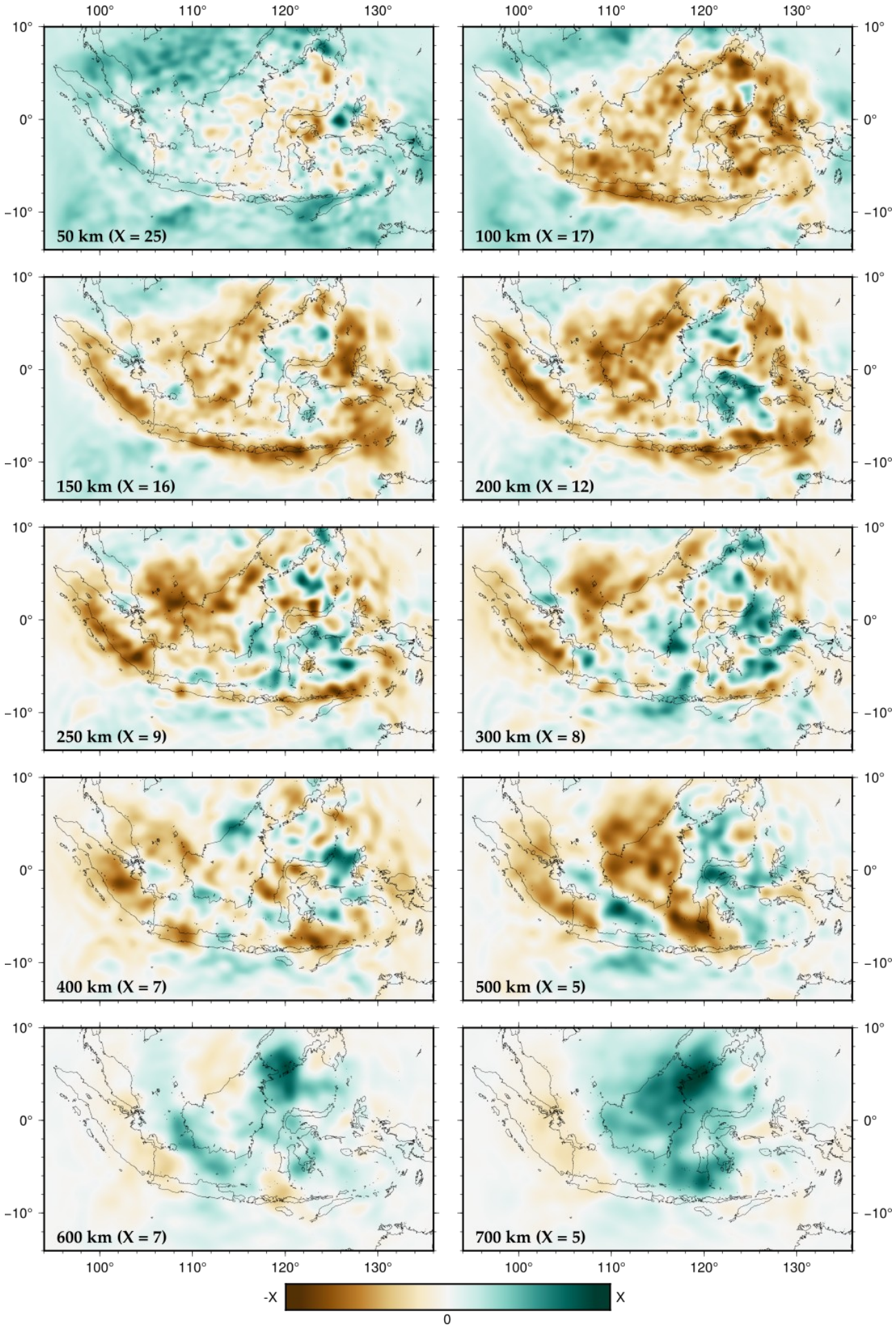

Figure S10: Slices through a radial anisotropy model derived from the FWI tomographic model, SASSY21, at various depths.